

Tensor Recovery Based on Tensor Equivalent Minimax-Concave Penalty

Hongbing Zhang, Xinyi Liu, Hongtao Fan, Yajing Li, Yinlin Ye

Abstract—Tensor recovery is an important problem in computer vision and machine learning. It usually uses the convex relaxation of tensor rank and l_0 norm, i.e., the nuclear norm and l_1 norm respectively, to solve the problem. It is well known that convex approximations produce biased estimators. In order to overcome this problem, a corresponding non-convex regularizer has been proposed to solve it. Inspired by matrix equivalent Minimax-Concave Penalty (EMCP), we propose and prove theorems of tensor equivalent Minimax-Concave Penalty (TEMCP). The tensor equivalent MCP (TEMCP) as a non-convex regularizer and the equivalent weighted tensor γ norm (EWTGN) which can represent the low-rank part are obtained. Both of them can realize weight adaptive. At the same time, we propose two corresponding adaptive models for two classical tensor recovery problems, low-rank tensor completion (LRTC) and tensor robust principal component analysis (TRPCA), and the optimization algorithm is based on alternating direction multiplier (ADMM). This novel iterative adaptive algorithm can produce more accurate tensor recovery effect. For the tensor completion model, multispectral image (MSI), magnetic resonance imaging (MRI) and color video (CV) data sets are considered, while for the tensor robust principal component analysis model, hyperspectral image (HSI) denoising under gaussian noise plus salt and pepper noise is considered. The proposed algorithm is superior to the state-of-arts method, and the algorithm is guaranteed to meet the reduction and convergence through experiments.

Index Terms—Tensor recovery, tensor equivalent MCP (TEMCP), equivalent weighted tensor γ norm (EWTGN), Low-rank tensor completion (LRTC), tensor robust principal component analysis (TRPCA), alternating direction method of multipliers (ADMM).

I. INTRODUCTION

WITH the continuous development of information technology, people are more and more interested in realistic data with high dimension and complex structure. As a higher dimensional generalization of vectors and matrices, tensors can better represent the complex properties of higher dimensional data. Therefore, tensors play an increasingly important role in many applications, such as color image/video (CI/CV) processing [1], [2], [3], [4], hyperspectral/multispectral image (HSI/MSI) processing [5], [6], [7], [8], magnetic resonance imaging (MRI) data recovery [9], [10], [11], [12], background

subtraction [13], [14], [15], [16], video rain stripe removal [17], [18] and signal reconstruction [19], [20].

Similar to the matrix recovery problem, the general method expresses the tensor recovery problem as follows:

$$\min_{\mathcal{X}} \text{rank}(\mathcal{X}) + \gamma L(\mathcal{X}, \mathcal{Y}), \quad (1)$$

where $\mathcal{Y} \in \mathbb{R}^{I_1 \times I_2 \times \dots \times I_N}$ is the observation, $L(\mathcal{X}, \mathcal{Y})$ is the loss function between \mathcal{X} and \mathcal{Y} , $\text{rank}(\mathcal{X})$ defines the tensor rank of \mathcal{X} and γ is the compromise parameter. In fact, tensors differ from matrices in that the definition of their rank is not unique. In the past decades, the most popular definitions of rank are CANDECOMP/PARAFAC(CP) rank based on CP decomposition [21], [22] and Tucker rank based on Tucker decomposition [23], [24], as well as tubal rank and multi-rank based on t-SVD [25]. Solving the CP rank problem of tensors is NP hard [26], which is not conducive to better application. The calculation of Tucker rank requires data to be fold and unfold, which will cause structural damage of data. Compared with CP rank and Tucker rank, the tubal rank and multiple rank obtained based on t-SVD can better ensure the data structure. But its tensor-tensor product limitation prevents it from being applied to higher order cases. Recently, Zheng et al. [27] proposed a new form of rank (N-tubal rank) based on tubal rank, adopting a new unfold method of higher-order tensors into third-order tensors in various directions. Benefiting from this, t-SVD can be applied to higher-order situations by solving multiple forms of third-order tensors. This approach not only makes good use of the properties of tensor tubal rank, but also enables t-SVD to be applied to higher order cases. Therefore, considering the excellent properties of N-tubal rank, we will also use N-tubal rank to construct the model we will propose in this paper.

There is no doubt that the development of computationally efficient algorithms to solve the problem (1) in the equation has great practical value. However, the rank optimization problem in the problem will lead to NP-hard problem, which will seriously affect the optimization of the problem. In general, people think about convex relaxation or non-convex relaxation. Convex relaxations are easier to solve, but they are known to produce biased estimates [28]. On the other hand, non-convex relaxation is more difficult, but correspondingly gives more accurate results [29], [30], [31],[32]. Recently, a matrix equivalent MCP (EMCP) method was proposed in [33] and applied to video foreground background separation task. This equivalent MCP method is novel, but when video data is processed by low rank plus sparse matrix, the data needs to be vectorized and then arranged into a matrix for processing.

This work was supported by the National Natural Science Foundation of China (Nos. 11701456, 11801452, 11571004), Fundamental Research Project of Natural Science in Shaanxi Province General Project (Youth) (Nos. 2019JQ-415, 2019JQ-196), the Initial Foundation for Scientific Research of Northwest A&F University (Nos.2452017219, 2452018017), and Innovation and Entrepreneurship Training Program for College Students of Shaanxi Province (S201910712132).

H. Zhang, X. Liu, H. Fan, Y. Li and Y. Ye are with the College of Science, Northwest A&F University, Yangling, Shaanxi 712100, China(e-mail: zhanghb@nwfufu.edu.cn; Lxy6x1@163.com; fanht17@nwfufu.edu.cn; hliyajing@163.com; 13314910376@163.com).

However, video data as a whole has a strong structure, and processing data through this vectorization reconstruction method will seriously damage the overall structure of data. In addition, video foreground background separation can be carried out by tensor robust principal component analysis, and the tensor method can protect the data structure well. Therefore, inspired by [33], we propose the method of tensor EMCP, and give relevant theorems and proofs. The proposed tensor EMCP method can realize parameter adaptation, which is more effective than the traditional MCP method. Furthermore, we study the two classical tensor recovery problems of tensor completeness and tensor robust principal component analysis, and establish two efficient adaptive models respectively. Through a large number of numerical experiments, it is shown that the proposed method can produce satisfactory results, and has obvious advantages over the comparison method in both vision and quantity.

To sum up, the main contributions of our paper are:

Firstly, a new theory called TEMCP is proposed for tensors with more complex structures than matrices. In this paper, theorems and theoretical proofs of EMCP and weighted GAMA norm of equivalent tensors are given, and some theoretical properties of the proposed theory are analyzed and discussed. Furthermore, in order to solve the model established by us based on this new theory, the corresponding operators and theoretical support of TEMCP and EWTGN are proposed respectively. (Relevant certificates are available in the appendix)

Secondly, our two typical problems of tensor recovery, tensor complete minimization problem and tensor robust principal component analysis, respectively is proposed and the optimization (corresponding) what the corresponding two kinds of adaptive model, and design the effective alternating direction multiplier method (ADMM) algorithm [34], [35] to solve each of these two kinds of classic problem. On this basis, the closed solution of each parameter update is deduced, which makes the algorithm run efficiently. Thus, the new tensor complete algorithm of TEMCPTC-Type-1 and TEMCPTC-Type-2 and the new tensor robust principal component analysis algorithm of TEMCPTRPCA-Type-1 and TEMCPTRPCA-Type-2 are obtained. The convergence of the two new algorithms is verified by experiments.

Thirdly, three different types of data, MSI, MRI and CV, were used to verify the experiment with complete tensors. A large number of numerical experiments show that the results obtained by the two complete adaptive methods are basically similar, and have obvious advantages over the comparison method in both visual and quantitative values. Considering that the noise of the data is not single in the actual situation, we study the mixed noise of the tensor robust principal component analysis. Experimental results show that our method still achieves better visual and quantitative results than the comparison method in the case of multiple noise damage combinations. The experimental synthesis of two classical tensor problems shows that our algorithm is better.

The summary of this article is as follows: Section II, some preliminary knowledge and background of the complete of tensors and matrices are given. The theorems of tensor EMCP and the theory of their properties are presented in

Section III. In Section IV, we give the corresponding proximal operators and theoretical proofs of TEMCP and EWTGN. The main results, including the proposed model and algorithm, are shown in Section V. The results of extensive experiments and discussion are presented in Section VI. Conclusions are drawn in section VII.

II. PRELIMINARIES

This section provides the basic knowledge of the proposed method. Firstly, we give the basic tensor notations.

A. Tensor Notations and Definitions

In this section, we give some basic notations and briefly introduce some definitions used throughout the paper. Generally, a lowercase letter and an uppercase letter denote a vector y and a matrix Y , respectively. An N th-order tensor is denoted by a calligraphic upper case letter $\mathcal{Y} \in \mathbb{R}^{I_1 \times I_2 \times \dots \times I_N}$ and y_{i_1, i_2, \dots, i_N} is its (i_1, i_2, \dots, i_N) -th element. The Frobenius norm of a tensor is defined as $\|\mathcal{Y}\|_F = (\sum_{i_1, i_2, \dots, i_N} y_{i_1, i_2, \dots, i_N}^2)^{1/2}$. For a three order tensor $\mathcal{Y} \in \mathbb{R}^{I_1 \times I_2 \times I_3}$. We use \mathcal{Y} to denote along each tubal of \mathcal{Y} , i.e., $\tilde{\mathcal{Y}} = \text{fft}(\mathcal{Y}, [], 3)$. The inverse DFT is computed by command ifft satisfying $\mathcal{Y} = \text{ifft}(\tilde{\mathcal{Y}}, [], 3)$. More often, the frontal slice $\mathcal{Y}(:, :, i)$ is denoted compactly as $\mathcal{Y}^{(i)}$.

Definition 1 (Mode- $k_1 k_2$ slices [27]): For an N th-order tensor $\mathcal{Y} \in \mathbb{R}^{I_1 \times I_2 \times \dots \times I_N}$, its mode- $k_1 k_2$ slices $(\mathcal{Y}^{(k_1 k_2)})$, $1 \leq k_1 < k_2 \leq N, k_1, k_2 \in \mathbb{Z}$ are two-dimensional sections, defined by fixing all but the mode- k_1 and the mode- k_2 indexes.

Definition 2 (Tensor Mode- k_1, k_2 Unfolding and Folding [27]): For an N th-order tensor $\mathcal{Y} \in \mathbb{R}^{I_1 \times I_2 \times \dots \times I_N}$, its mode- $k_1 k_2$ unfolding is a three order tensor denoted by $\mathcal{Y}_{(k_1 k_2)} \in \mathbb{R}^{I_{k_1} \times I_{k_2} \times \prod_{s \neq k_1, k_2} I_s}$, the frontal slices of which are the lexicographic orderings of the mode- $k_1 k_2$ slices of \mathcal{Y} . Mathematically, the (i_1, i_2, \dots, i_N) -th element of \mathcal{Y} maps to the (i_{k_1}, i_{k_2}, j) -th element of $\mathcal{Y}_{(k_1 k_2)}$, where

$$j = 1 + \sum_{s=1, s \neq k_1, s \neq k_2}^N (i_s - 1)J_s \quad \text{with} \quad J_s = \prod_{m=1, m \neq k_1, m \neq k_2}^{s-1} I_m. \quad (2)$$

The mode- $k_1 k_2$ unfolding operator and its inverse operation are respectively denoted as $\mathcal{Y}_{(k_1 k_2)} := \text{t-unfold}(\mathcal{Y}, k_1, k_2)$ and $\mathcal{Y} := \text{t-fold}(\mathcal{Y}_{(k_1 k_2)}, k_1, k_2)$.

For a three order tensor $\mathcal{Y} \in \mathbb{R}^{I_1 \times I_2 \times I_3}$, the block circulation operation is defined as

$$\text{bcirc}(\mathcal{Y}) := \begin{pmatrix} Y^{(1)} & Y^{(3)} & \dots & Y^{(2)} \\ Y^{(2)} & Y^{(1)} & \dots & Y^{(3)} \\ \vdots & \vdots & \ddots & \vdots \\ Y^{(3)} & Y^{(3-1)} & \dots & Y^{(1)} \end{pmatrix} \in \mathbb{R}^{I_1 I_3 \times I_2 I_3}.$$

The block diagonalization operation and its inverse operation are defined as

$$\text{bdiag}(\mathcal{Y}) := \begin{pmatrix} Y^{(1)} & & & \\ & Y^{(2)} & & \\ & & \ddots & \\ & & & Y^{(3)} \end{pmatrix} \in \mathbb{R}^{I_1 I_3 \times I_2 I_3},$$

$$\text{bdfold}(\text{bdiag}(\mathcal{Y})) := \mathcal{Y}.$$

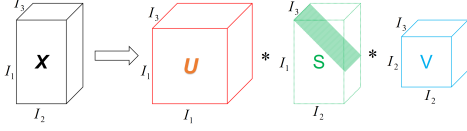


Fig. 1. An illustration of the t-SVD of an $I_1 \times I_2 \times I_3$ tensor

The block vectorization operation and its inverse operation are defined as

$$bvec(\mathcal{Y}) := \begin{pmatrix} Y^{(1)} \\ Y^{(2)} \\ \vdots \\ Y^{(I_3)} \end{pmatrix} \in \mathbb{R}^{I_1 I_3 \times I_2}, \quad bvfold(bvec(\mathcal{Y})) := \mathcal{Y}.$$

Definition 3 (T-product [36]): Let $\mathcal{A} \in \mathbb{R}^{I_1 \times I_2 \times I_3}$ and $\mathcal{B} \in \mathbb{R}^{I_2 \times J \times I_3}$. Then the t-product $\mathcal{A} * \mathcal{B}$ is defined to be a tensor of size $I_1 \times J \times I_3$,

$$\mathcal{A} * \mathcal{B} := bvfold(bcirc(\mathcal{A})bvec(\mathcal{B})).$$

Since that circular convolution in the spatial domain is equivalent to multiplication in the Fourier domain, the T-product between two tensors $\mathcal{C} = \mathcal{A} * \mathcal{B}$ is equivalent to

$$\bar{\mathcal{C}} = bdfold(bdiag(\bar{\mathcal{A}})bdiag(\bar{\mathcal{B}})).$$

Definition 4 (Tensor conjugate transpose [36]): The conjugate transpose of a tensor $\mathcal{A} \in \mathbb{C}^{I_1 \times I_2 \times I_3}$ is the tensor $\mathcal{A}^H \in \mathbb{C}^{I_2 \times I_1 \times I_3}$ obtained by conjugate transposing each of the frontal slices and then reversing the order of transposed frontal slices 2 through I_3 .

Definition 5 (identity tensor [36]): The identity tensor $\mathcal{I} \in \mathbb{R}^{I_1 \times I_1 \times I_3}$ is the tensor whose first frontal slice is the $I_1 \times I_1$ identity matrix, and whose other frontal slices are all zeros.

It is clear that $bcirc(\mathcal{I})$ is the $I_1 I_3 \times I_1 I_3$ identity matrix. So it is easy to get $\mathcal{A} * \mathcal{I} = \mathcal{A}$ and $\mathcal{I} * \mathcal{A} = \mathcal{A}$.

Definition 6 (orthogonal tensor [36]): A tensor $\mathcal{Q} \in \mathbb{R}^{I_1 \times I_1 \times I_3}$ is orthogonal if it satisfied

$$\mathcal{Q} * \mathcal{Q}^H = \mathcal{Q}^H * \mathcal{Q} = \mathcal{I}.$$

Definition 7 (F-diagonal Tensor [36]): A tensor is called f-diagonal if each of its frontal slices is a diagonal matrix.

Theorem 1 (t-SVD [37]): Let $\mathcal{X} \in \mathbb{R}^{I_1 \times I_2 \times I_3}$ be a three order tensor, then it can be factored as

$$\mathcal{X} = \mathcal{U} * \mathcal{S} * \mathcal{V}^H,$$

where $\mathcal{U} \in \mathbb{R}^{I_1 \times I_1 \times I_3}$ and $\mathcal{V} \in \mathbb{R}^{I_2 \times I_2 \times I_3}$ are orthogonal tensors, and $\mathcal{S} \in \mathbb{R}^{I_1 \times I_2 \times I_3}$ is an f-diagonal tensor. The t-SVD scheme is illustrated in Fig.1, and its computation is given in Algorithm 1.

Definition 8 (tensor tubal-rank and multi-rank [25]): The tubal-rank of a tensor $\mathcal{Y} \in \mathbb{R}^{I_1 \times I_2 \times I_3}$, denoted as $rank_t(\mathcal{Y})$, is defined to be the number of non-zero singular tubes of \mathcal{S} , where \mathcal{S} comes from the t-SVD of \mathcal{Y} : $\mathcal{Y} = \mathcal{U} * \mathcal{S} * \mathcal{V}^H$. That is

$$rank_t(\mathcal{Y}) = \#\{i : \mathcal{S}(i, :, :) \neq \mathbf{0}\}. \quad (3)$$

Algorithm 1 t-SVD [37]

Input: $\mathcal{Y} \in \mathbb{R}^{I_1 \times I_2 \times I_3}$

Output: t-SVD components \mathcal{U} , \mathcal{S} and \mathcal{V} of \mathcal{A} .

Compute $\bar{\mathcal{A}} = fft(\mathcal{A}, [], 3)$.

Compute each frontal slice of $\bar{\mathcal{U}}$, $\bar{\mathcal{S}}$, and $\bar{\mathcal{V}}$ from $\bar{\mathcal{A}}$ by

for $i = 1, \dots, \lceil \frac{I_3+1}{2} \rceil$ **do**

$$[\bar{\mathcal{U}}^{(i)}, \bar{\mathcal{S}}^{(i)}, \bar{\mathcal{V}}^{(i)}] = SVD(\bar{\mathcal{A}}^{(i)});$$

end for

for $i = \lceil \frac{I_3+1}{2} \rceil + 1, \dots, I_3$ **do**

$$[\bar{\mathcal{U}}^{(i)}, \bar{\mathcal{S}}^{(i)}, \bar{\mathcal{V}}^{(i)}] = SVD(\bar{\mathcal{A}}^{(i)});$$

$$\bar{\mathcal{U}}^{(i)} = conj(\bar{\mathcal{U}}^{(I_3-i+2)});$$

$$\bar{\mathcal{S}}^{(i)} = \bar{\mathcal{S}}^{(I_3-i+2)};$$

$$\bar{\mathcal{V}}^{(i)} = conj(\bar{\mathcal{V}}^{(I_3-i+2)});$$

end for

Compute $\mathcal{U} = ifft(\bar{\mathcal{U}}, [], 3)$, $\mathcal{S} = ifft(\bar{\mathcal{S}}, [], 3)$, and $\mathcal{V} = ifft(\bar{\mathcal{V}}, [], 3)$.

The tensor multi-rank of $\mathcal{Y} \in \mathbb{R}^{I_1 \times I_2 \times I_3}$ is a vector, denoted as $rank_r(\mathcal{Y}) \in \mathbb{R}^{I_3}$, with the i -th element equals to the rank of i -th frontal slice of \mathcal{Y} .

Definition 9 (tensor nuclear norm (TNN)): The tensor nuclear norm of a tensor $\mathcal{Y} \in \mathbb{R}^{I_1 \times I_2 \times I_3}$, denoted as $\|\mathcal{Y}\|_{TNN}$, is defined as the sum of the singular values of all the frontal slices of \mathcal{Y} , i.e.,

$$\|\mathcal{Y}\|_{TNN} := \sum_{i=1}^{I_3} \|\bar{\mathcal{Y}}^{(i)}\|_* \quad (4)$$

where $\bar{\mathcal{Y}}^{(i)}$ is the i -th frontal slice of $\bar{\mathcal{Y}}$, with $\bar{\mathcal{Y}} = fft(\mathcal{Y}, [], 3)$.

Definition 10 (N-tubal rank [27]): The N-tubal rank of an Nth-order tensor $\mathcal{Y} \in \mathbb{R}^{I_1 \times I_2 \times \dots \times I_N}$ is defined as a vector, the elements of which contain the tubal rank of all mode- $k_1 k_2$ unfolding tensors, i.e.,

$$\begin{aligned} N - rank_t(\mathcal{Y}) := & (rank_t(\mathcal{Y}_{(12)}), rank_t(\mathcal{Y}_{(13)}), \dots, \\ & rank_t(\mathcal{Y}_{(1N)}), rank_t(\mathcal{Y}_{(23)}), \dots, rank_t(\mathcal{Y}_{(2N)}), \dots, \\ & rank_t(\mathcal{Y}_{(N-1N)})) \in \mathbb{R}^{N(N-1)/2}. \end{aligned} \quad (5)$$

B. EQUIVALENT MCP (EMCP)

In this section, we first introduce the definition of the MCP function.

Definition 11 (Scalar MCP [38]): Let $\lambda > 0, \gamma > 1$. The scalar MCP $h_\gamma : \mathbb{R} \rightarrow \mathbb{R}_{\geq 0}$ is defined as

$$h_{\gamma, \lambda}(y) = \begin{cases} \lambda|y| - \frac{y^2}{2\gamma}, & |y| \leq \gamma\lambda, \\ \frac{y^2}{2\gamma}, & |y| \geq \gamma\lambda. \end{cases} \quad (6)$$

Definition 12 (Vector MCP [38]): Let $y \in \mathbb{R}^n$ and $\lambda > 0, \gamma > 1$. The vector MCP $h_{\gamma, \lambda} : \mathbb{R}^n \rightarrow \mathbb{R}_{\geq 0}$ is defined as

$$h_{\gamma, \lambda}(y) = \sum_{i=1}^n h_{\gamma, \lambda}(y_i), \quad (7)$$

where y_i denotes the i th entry of the vector y and $h_{\gamma, \lambda}(y_i)$ is defined in (6).

Definition 13 (Matrix MCP [39]): Let $Y \in \mathbb{R}^{m \times n}$ and $\lambda > 0, \gamma > 1$. The matrix MCP $h_{\gamma, \lambda} : \mathbb{R}^{m \times n} \rightarrow \mathbb{R}_{\geq 0}$ is defined as

$$h_{\gamma, \lambda}(Y) = \sum_{i=1}^m \sum_{j=1}^n h_{\gamma, \lambda}(Y_{ij}), \quad (8)$$

where Y_{ij} denotes the (i, j) element of Y , and $h_{\gamma, \lambda}$ is also defined in (6).

We next present definitions pertaining to quantification of the low-rank property of a matrix.

Definition 14 (Weighted nuclear norm [40]): Consider a rank- r matrix $Y \in \mathbb{R}^{m \times n}$ with the SVD: $Y = U \text{diag}(\sigma) V^T$, where $\sigma = [\sigma_1, \sigma_2, \dots, \sigma_r]$ is the vector of singular values. The weighted nuclear norm of Y , denoted by $\|Y\|_{\omega, *}$, is defined as:

$$\|Y\|_{\omega, *} = \sum_{i=1}^r \omega_i \sigma_i = \|\sigma\|_{\omega, 1}. \quad (9)$$

where $\omega \in \mathbb{R}_{\geq 0}^r$ is a non-negative weight vector with the i th entry ω_i and $\|\sigma\|_{\omega, 1}$ denotes the weighted l_1 -norm of the vector of singular values.

The weighted nuclear norm is convex in the singular values. Considering the vector MCP instead of the weighted l_1 -norm gives rise to the matrix γ -norm (MGN) [38]:

Definition 15 (Matrix γ -norm [39]): The γ -norm of a rank- r matrix $Y \in \mathbb{R}^{m \times n}$, denoted by $\|Y\|_{\gamma, \lambda}$, is defined as

$$\|Y\|_{\gamma, \lambda} = h_{\gamma, \lambda}(\sigma) = \sum_{i=1}^r h_{\gamma, \lambda}(\sigma_i). \quad (10)$$

Similarly, the weighted matrix γ -norm (WMGN) is a generalization of WMCP for matrices and is defined as follows.

Definition 16 (Weighted matrix γ -norm [33]): The weighted matrix γ -norm of $Y \in \mathbb{R}^{m \times n}$, denoted by $\|Y\|_{\gamma, \lambda}$, is defined in terms of the singular values $\{\sigma_i, i = 1, 2, \dots, r\}$ as follows:

$$\|Y\|_{\gamma, \lambda} = h_{\gamma, \lambda}(\sigma) = \sum_{i=1}^r h_{\gamma, \lambda_i}(\sigma_i). \quad (11)$$

where $r = \min(m, n)$ denotes the maximum rank of Y .

Recently, the equivalent MCP form related to the above definition has been proposed, as follows:

Theorem 2 (Scalar EMCP [33]): Let $\lambda > 0, \gamma > 1$ and $y \in \mathbb{R}$. The scalar MCP $h_{\gamma, \lambda} : \mathbb{R} \rightarrow \mathbb{R}_{\geq 0}$ is the solution of the following optimization problem:

$$h_{\gamma, \lambda}(y) = \min_{\omega \in \mathbb{R}_{\geq 0}} \left\{ \omega |y| + \frac{\gamma}{2} (\omega - \lambda)^2 \right\}. \quad (12)$$

Theorem 3 (Vector EMCP [33]): Let $\gamma > 1, \omega \in \mathbb{R}_{\geq 0}^n, \lambda \in \mathbb{R}_{\geq 0}^n$ and $y \in \mathbb{R}^n$. The vector MCP is the solution of the following optimization problem:

$$h_{\gamma, \lambda}(y) = \min_{\omega \in \mathbb{R}_{\geq 0}^n} \left\{ \|y\|_{\omega, 1} + \frac{\gamma}{2} \|\omega - \lambda\|_2^2 \right\}, \quad (13)$$

where $\|y\|_{\omega, 1}$ denotes the weighted l_1 -norm of y defined as

$$\|y\|_{\omega, 1} = \sum_{i=1}^n \omega_i |y_i|, \quad \omega_i \geq 0,$$

and $\{\omega_i, i = 1, 2, \dots, n\}$ denote the weights.

Theorem 4 (Matrix EMCP [33]): Let $\gamma > 1, \Omega \in \mathbb{R}_{\geq 0}^{m \times n}, \Lambda \in \mathbb{R}_{\geq 0}^{m \times n}$ and $Y \in \mathbb{R}^{m \times n}$. The matrix MCP is the solution of the following optimization problem:

$$h_{\gamma, \Lambda}(Y) = \min_{\Omega \in \mathbb{R}_{\geq 0}^{m \times n}} \left\{ \|Y\|_{\Omega, 1} + \frac{\gamma}{2} \|\Omega - \Lambda\|_2^2 \right\}, \quad (14)$$

where $\|Y\|_{\Omega, 1}$ denotes the weighted l_1 -norm of the matrix Y defined as

$$\|Y\|_{\Omega, 1} = \sum_{i=1}^m \sum_{j=1}^n \Omega_{ij} |Y_{ij}|,$$

where $\{\Omega_{ij} \geq 0, i = 1, 2, \dots, m, j = 1, 2, \dots, n\}$ denote the weights.

Theorem 5 (Equivalent matrix γ -norm (EMGN) [33]): Consider a rank- r matrix $Y \in \mathbb{R}^{m \times n}$ with the SVD: $Y = U \text{diag}(\sigma) V^T$, where $\sigma = [\sigma_1, \sigma_2, \dots, \sigma_r]^T$. Let $\{\omega, \lambda\} \in \mathbb{R}_{\geq 0}^r$, and $\gamma > 1$. The matrix γ -norm (EMGN) is obtained equivalently as

$$\|Y\|_{\gamma, \lambda} = \min_{\omega \in \mathbb{R}_{\geq 0}^r} \left\{ \|Y\|_{\omega, *} + \frac{\gamma}{2} \|\omega - \lambda\|_2^2 \right\}, \quad (15)$$

where $\|Y\|_{\omega, 1} = \sum_{i=1}^r \omega_i \sigma_i$ is the weighted nuclear-norm.

III. TENSOR EQUIVALENT MCP (TEMCP)

Definition 17 (Tensor MCP): Let $\mathcal{Y} \in \mathbb{R}^{I_1 \times I_2 \times \dots \times I_N}$ and $\bar{\lambda} \in \mathbb{R}_{\geq 0}^{I_1 \times I_2 \times \dots \times I_N}, \gamma > 1$. The tensor MCP $h_{\gamma, \bar{\lambda}} : \mathbb{R}^{I_1 \times I_2 \times \dots \times I_N} \rightarrow \mathbb{R}_{\geq 0}$ is defined as

$$h_{\gamma, \bar{\lambda}}(\mathcal{Y}) = \sum_{i_1=1}^{I_1} \sum_{i_2=1}^{I_2} \dots \sum_{i_N=1}^{I_N} h_{\gamma, \bar{\lambda}_{i_1, i_2, \dots, i_N}}(\mathcal{Y}_{i_1, i_2, \dots, i_N}), \quad (16)$$

where $\mathcal{Y}_{i_1, i_2, \dots, i_N}$ denotes the (i_1, i_2, \dots, i_N) -th element of \mathcal{Y} , and $h_{\gamma, \bar{\lambda}}$ is defined in (6).

Definition 18 (Weighted tensor γ -norm (WTGN)): The weighted tensor γ -norm of $\mathcal{Y} \in \mathbb{R}^{I_1 \times I_2 \times I_3}$, denoted by $\|\mathcal{Y}\|_{\gamma, \bar{\lambda}}$, is defined as follows:

$$\|\mathcal{Y}\|_{\gamma, \bar{\lambda}} = \sum_{i=1}^{I_3} \|\tilde{\mathcal{Y}}^{(i)}\|_{\gamma, \bar{\lambda}_i} = \sum_{i=1}^{I_3} \sum_{j=1}^R h_{\gamma, \bar{\lambda}_{i, j}}(\sigma_j(\tilde{\mathcal{Y}}^{(i)})). \quad (17)$$

where $R = \min(I_1, I_2)$.

Theorem 6 (Tensor EMCP): Let $\gamma > 1, \mathcal{W}, \bar{\lambda} \in \mathbb{R}_{\geq 0}^{I_1 \times I_2 \times \dots \times I_N}$ and $\mathcal{Y} \in \mathbb{R}^{I_1 \times I_2 \times \dots \times I_N}$. The tensor MCP is the solution to the optimization:

$$h_{\gamma, \bar{\lambda}}(\mathcal{Y}) = \min_{\mathcal{W}} \left\{ \|\mathcal{Y}\|_{\mathcal{W}, 1} + \frac{\gamma}{2} \|\mathcal{W} - \bar{\lambda}\|_F^2 \right\}, \quad (18)$$

where $\|\mathcal{Y}\|_{\mathcal{W}, 1}$ denotes the weighted l_1 -norm of the tensor \mathcal{Y} defined as

$$\|\mathcal{Y}\|_{\mathcal{W}, 1} = \sum_{i_1=1}^{I_1} \sum_{i_2=1}^{I_2} \dots \sum_{i_N=1}^{I_N} \mathcal{W}_{i_1, i_2, \dots, i_N} \mathcal{Y}_{i_1, i_2, \dots, i_N} \quad (19)$$

where \mathcal{W} is weight tensor.

Proof: The proof is provided in Appendix A. ■

Theorem 7 (Equivalent Weighted Tensor γ -norm (EWTGN)): For a third-order tensor $\mathcal{Y} \in \mathbb{R}^{I_1 \times I_2 \times I_3}$, its SVD is decomposed into $\mathcal{Y} = \mathcal{U} * \mathcal{S} * \mathcal{V}$, where $\mathcal{S} \in \mathbb{R}^{R \times R \times I_3}$ and $R = \min\{I_1, I_2\}$.

Let $W, \bar{\Lambda} \in \mathbb{R}_{\geq 0}^{R \times I_3}$, and $\gamma > 1$. The weighted tensor γ -norm is obtained equivalently as

$$\|\mathcal{Y}\|_{\gamma, \bar{\Lambda}} = \min_W \left\{ \sum_{i_3=1}^{I_3} \|\bar{\mathcal{Y}}^{(i_3)}\|_{W_{(:,i_3),*}} + \frac{\gamma}{2} \|W - \bar{\Lambda}\|_F^2 \right\} \quad (20)$$

where $\|\bar{\mathcal{Y}}^{(i_3)}\|_{W_{(:,i_3),*}} = \sum_{j=1}^R W_{j,i_3} \sigma_j(\bar{\mathcal{Y}}^{(i_3)})$ is the weighted nuclear-norm of i_3 -th slice of $\bar{\mathcal{Y}}$.

Proof: The proof is provided in Appendix B. ■

Unlike the l_1 penalty or the nuclear norm penalty, the tensor MCP (16), WTGN (17), tensor EMCP (18), and EWTGN (20) do not satisfy the triangle inequality. Some important properties satisfied by the tensor EMCP and EWTGN are given below.

Proposition 1: The tensor EMCP $h_{\gamma, \bar{\Lambda}}(\mathcal{Y})$ defined in (16) satisfies the following properties:

(a) **Non-negativity:** The tensor EMCP is non-negative, i.e., $h_{\gamma, \bar{\Lambda}}(\mathcal{Y}) \geq 0$. The equality holds if and only if \mathcal{Y} is the null tensor.

(b) **Concavity:** $h_{\gamma, \bar{\Lambda}}(\mathcal{Y})$ is concave in the modulus of the elements of \mathcal{Y} .

(c) **Boundedness:** The tensor EMCP is upper-bounded by the weighted l_1 norm, i.e., $h_{\gamma, \bar{\Lambda}}(\mathcal{Y}) \leq \|\mathcal{Y}\|_{\bar{\Lambda}, 1}$.

(d) **Asymptotic l_1 property:** The tensor EMCP approaches the weighted l_1 norm asymptotically, i.e., $\lim_{\gamma \rightarrow \infty} h_{\gamma, \bar{\Lambda}}(\mathcal{Y}) = \|\mathcal{Y}\|_{\bar{\Lambda}, 1}$

Proof: The proof is provided in Appendix C. ■

Proposition 2: The EWTGN defined in (20) satisfies the following properties:

(a) **Non-negativity:** The EWTGN is non-negative, i.e., $\|\mathcal{Y}\|_{\gamma, \bar{\Lambda}} \geq 0$. The equality holds if and only if \mathcal{Y} is the null tensor.

(b) **Concavity:** $\|\mathcal{Y}\|_{\gamma, \bar{\Lambda}}$ is concave in the modulus of the elements of \mathcal{Y} .

(c) **Boundedness:** The EWTGN is upper-bounded by the weighted nuclear norm, i.e., $\|\mathcal{Y}\|_{\gamma, \bar{\Lambda}} \leq \|\mathcal{Y}\|_{\bar{\Lambda}, *}$.

(d) **Asymptotic nuclear norm property:** The EWTGN approaches the weighted nuclear norm asymptotically, i.e., $\lim_{\gamma \rightarrow \infty} \|\mathcal{Y}\|_{\gamma, \bar{\Lambda}} = \|\mathcal{Y}\|_{\bar{\Lambda}, *}$.

(e) **Unitary invariance:** The EWTGN is unitary invariant, i.e., $\|\mathcal{U} * \mathcal{Y} * \mathcal{V}\|_{\gamma, \bar{\Lambda}} = \|\mathcal{Y}\|_{\gamma, \bar{\Lambda}}$, for unitary tensor \mathcal{U} and \mathcal{V} .

Proof: The proof is provided in Appendix D. ■

IV. PROXIMAL OPERATORS FOR TENSOR EMCP AND EWTGN

In this section, we present the proximal operators for the tensor EMCP and EWTGN. The proximal operators corresponding to scalar EMCP, vector EMCP, matrix EMCP, and EMGN are available in the literature [33]. We derive the proximal operators for the tensor equivalent representations developed in this paper, namely, tensor EMCP (18), and EWTGN (20). The proofs are provided in the supplement document.

Theorem 8 (Proximal operator for tensor EMCP): Consider the tensor EMCP given in (18). Its proximal operator denoted by $P_{\gamma, \bar{\Lambda}} : \mathbb{R}^{I_1 \times I_2 \times \dots \times I_N} \rightarrow \mathbb{R}^{I_1 \times I_2 \times \dots \times I_N}$, $\gamma > 1, \bar{\Lambda} \in \mathbb{R}_{\geq 0}^{I_1 \times I_2 \times \dots \times I_N}$ and defined as follows:

$$P_{\gamma, \bar{\Lambda}}(\mathcal{Y}) = \arg \min_{\mathcal{G}} \left\{ \frac{\rho}{2} \|\mathcal{G} - \mathcal{Y}\|_F^2 + h_{\gamma, \bar{\Lambda}}(\mathcal{G}) \right\}, \quad (21)$$

is given by

$$P_{\gamma, \bar{\Lambda}}(\mathcal{Y}) = \min(|\mathcal{Y}|, \max(\frac{\tau}{\tau-1} (|\mathcal{Y}| - \frac{\bar{\Lambda}}{\rho}), \mathbf{0})) \odot \text{sign}(\mathcal{Y}). \quad (22)$$

where $\tau = \rho\gamma$.

Proof: The proof is provided in Appendix E. ■

Theorem 9 (Proximal operator for EWTGN): Consider the tensor EMCP given in (20). Its proximal operator denoted by $S_{\gamma, \bar{\Lambda}} : \mathbb{R}^{I_1 \times I_2 \times I_3} \rightarrow \mathbb{R}^{I_1 \times I_2 \times I_3}$, $\gamma > 1$, $\bar{\Lambda} \in \mathbb{R}_{\geq 0}^{R \times I_3}$, $R = \min\{I_1, I_2\}$ and defined as follows:

$$S_{\gamma, \bar{\Lambda}}(\mathcal{Y}) = \arg \min_{\mathcal{L}} \left\{ \frac{\rho}{2} \|\mathcal{L} - \mathcal{Y}\|_F^2 + \|\mathcal{L}\|_{\gamma, \bar{\Lambda}} \right\}, \quad (23)$$

is given by

$$S_{\gamma, \bar{\Lambda}}(\mathcal{Y}) = \mathcal{U} * \mathcal{S}_1 * \mathcal{V}^H. \quad (24)$$

where \mathcal{U} and \mathcal{V} derive from the t-SVD of $\mathcal{Y} = \mathcal{U} * \mathcal{S}_2 * \mathcal{V}^H$. More importantly, the i th front slice of DFT of \mathcal{S}_1 and \mathcal{S}_2 , i.e., $\bar{\mathcal{S}}_1^{(i)} = \sigma(\bar{\mathcal{L}}^{(i)})$ and $\bar{\mathcal{S}}_2^{(i)} = \sigma(\bar{\mathcal{Y}}^{(i)})$, has the following relationship

$$\sigma(\bar{\mathcal{L}}^{(i)}) = \min\{\sigma(\bar{\mathcal{Y}}^{(i)}), \max\{\frac{\tau(\sigma(\bar{\mathcal{Y}}^{(i)}) - \frac{\bar{\Lambda}_{(:,i)}}{\rho})}{\tau-1}, 0\}\}, \quad (25)$$

where $\tau = \gamma\rho$.

Proof: The proof is provided in Appendix F. ■

The proximal operators are crucial in the derivation of the tensor recovery algorithms that will be developed in the following section.

V. TENSOR EQUIVALENT MCP MODELS AND SOLVING ALGORITHMS

A. TEMCP LRTC model

The optimization problem of LRTC takes the following form:

$$\min_{\mathcal{X}} \sum_{1 \leq l_1 < l_2 \leq N} \alpha_{l_1 l_2} \|\mathcal{X}_{(l_1 l_2)}\|_{\gamma, \bar{\Lambda}} \quad \text{s.t.} \quad \mathcal{P}_{\Omega}(\mathcal{X} - \mathcal{Z}) = 0, \quad (26)$$

We solve the problem within the ADMM framework and rely on the proximal operators given in Theorem 9 to derive the optimization algorithms.

1) *Adaptive TEMCP LRTC-Type-1:* An adaptive variant of the problem stated in (26) takes the following form:

$$\min_{\mathcal{X}, \mathcal{Y}, \bar{\Lambda}, W, Q} \sum_{1 \leq l_1 < l_2 \leq N} \alpha_{l_1 l_2} \|\mathcal{Y}_{l_1 l_2}(l_1 l_2)\|_{\gamma, \bar{\Lambda}_{l_1 l_2}} + \frac{\rho_{l_1 l_2}}{2} \|\mathcal{X} - \mathcal{Y}_{l_1 l_2} + \frac{Q_{l_1 l_2}}{\rho_{l_1 l_2}}\|_F^2 \quad \text{s.t.} \quad \mathcal{P}_{\Omega}(\mathcal{X} - \mathcal{Z}) = 0 \quad (27)$$

where \mathcal{Y} and Q are tensor sets; $\bar{\Lambda}$ and W are matrix sets; $\{\mathcal{Y}_{l_1 l_2} = \mathcal{X}\}_{1 \leq l_1 < l_2 \leq N}$; $\{Q\}_{1 \leq l_1 < l_2 \leq N}$ are Lagrangian multiplier; $\{\bar{\Lambda}, W\}_{1 \leq l_1 < l_2 \leq N} \in \mathbb{R}^{R \times I_3}$ are MCP parameter set and weight set, respectively; $\{\rho_{l_1 l_2}\}_{1 \leq l_1 < l_2 \leq N} > 0$ are the augmented Lagrangian parameter; $\alpha_{l_1 l_2} \geq 0$ are weights and $\sum_{1 \leq l_1 < l_2 \leq N} \alpha_{l_1 l_2} = 1$.

Within the framework of the ADMM, \mathcal{X} , \mathcal{Y} , $\bar{\Lambda}$, W , Q are updated alternately in the order of $\mathcal{Y} \rightarrow W \rightarrow \bar{\Lambda} \rightarrow \mathcal{X} \rightarrow Q$.

For convenience, we will mark the updated variable as $(\cdot)^+$. The update equations are derived in the following.

Update \mathcal{Y} : Fix other variables, and the corresponding optimization instructions are as follows:

$$\mathcal{Y}_{l_1 l_2}^+ = \min_{\mathcal{Y}_{l_1 l_2}} \alpha_{l_1 l_2} \|\mathcal{Y}_{l_1 l_2(l_1 l_2)}\|_{\gamma, \bar{\Lambda}_{l_1 l_2}} + \frac{\rho_{l_1 l_2}}{2} \|\mathcal{X} - \mathcal{Y}_{l_1 l_2} + \frac{\mathcal{Q}_{l_1 l_2}}{\rho_{l_1 l_2}}\|_F^2.$$

Theorem 9 provides the following solution to the above problem:

$$\mathcal{Y}_{l_1 l_2}^+ = S_{\frac{\gamma \rho_{l_1 l_2}}{\alpha_{l_1 l_2}}, \frac{\bar{\Lambda}_{l_1 l_2} \rho_{l_1 l_2}}{\alpha_{l_1 l_2}}} (\mathcal{X} + \frac{\mathcal{Q}_{l_1 l_2}}{\rho_{l_1 l_2}}). \quad (28)$$

where S denotes the proximal operator defined in (24).

Update W : Retaining only those components in $\mathcal{Y}_{l_1 l_2}$ in (28) that depend on $W_{l_1 l_2}$, we write

$$W_{l_1 l_2}^+ = \min_{W_{l_1 l_2}} \sum_{i_3=1}^{I_3} \|\bar{\mathcal{Y}}_{l_1 l_2}^{(i_3)}\|_{W_{l_1 l_2(:, i_3)}, * } + \frac{\gamma}{2} \|W_{l_1 l_2} - \bar{\Lambda}_{l_1 l_2}\|_F^2. \quad (29)$$

which has the following closed-form solution:

$$W_{l_1 l_2(:, i_3)}^+ = \max(\bar{\Lambda}_{l_1 l_2(:, i_3)} - \frac{\sigma(\bar{\mathcal{Y}}_{l_1 l_2}^{(i_3)})}{\gamma}, 0). \quad (30)$$

Update $\bar{\Lambda}$: The update for $\bar{\Lambda}_{l_1 l_2}$ turns out to be straightforward as the only term of $\mathcal{Y}_{l_1 l_2}$ in (28) that depends on $\bar{\Lambda}_{l_1 l_2}$ is a quadratic:

$$\bar{\Lambda}_{l_1 l_2}^+ = \min_{\bar{\Lambda}_{l_1 l_2}} \|W_{l_1 l_2} - \bar{\Lambda}_{l_1 l_2}\|_F^2 = W_{l_1 l_2}^+. \quad (31)$$

Update \mathcal{X} : The closed form of \mathcal{X} can be derived by setting the derivative of (28) with respect to zero. We can now update \mathcal{X} by the following equation:

$$\mathcal{X}^+ = \mathcal{P}_{\Omega^c} \left(\frac{\sum_{1 \leq l_1 < l_2 \leq N} \rho_{l_1 l_2} (\mathcal{Y}_{l_1 l_2} - \frac{\mathcal{Q}_{l_1 l_2}}{\rho_{l_1 l_2}})}{\sum_{1 \leq l_1 < l_2 \leq N} \rho_{l_1 l_2}} \right) + \mathcal{P}_{\Omega}(\mathcal{Z}) \quad (32)$$

Update \mathcal{Q} : Finally, multipliers $\mathcal{Q}_{l_1 l_2}$ are updated as follows:

$$\mathcal{Q}_{l_1 l_2}^+ = \mathcal{Q}_{l_1 l_2} + \rho_{l_1 l_2} (\mathcal{X} - \mathcal{Y}_{l_1 l_2}). \quad (33)$$

The optimization steps of TEMCPLRTC-Type-1 formulation are listed in Algorithm 2.

2) *Adaptive TEMCP LRTC-Type-2:* Another adaptive variant of the problem stated in (26) takes the following form:

$$\begin{aligned} \min_{\mathcal{X}, \mathcal{Y}, W, \mathcal{Q}} \quad & \sum_{1 \leq l_1 < l_2 \leq N} \alpha_{l_1 l_2} \sum_{i_3=1}^{I_3} \|\bar{\mathcal{Y}}_{l_1 l_2}^{(i_3)}\|_{W_{l_1 l_2(:, i_3)}, * } \\ & + \frac{\gamma}{2} \|W_{l_1 l_2} - \bar{\Lambda}_{l_1 l_2}\|_F^2 + \frac{\rho_{l_1 l_2}}{2} \|\mathcal{X} - \mathcal{Y}_{l_1 l_2} + \frac{\mathcal{Q}_{l_1 l_2}}{\rho_{l_1 l_2}}\|_F^2 \\ \text{s.t.} \quad & \mathcal{P}_{\Omega}(\mathcal{X} - \mathcal{Z}) = 0, \end{aligned} \quad (34)$$

where \mathcal{Y} , \mathcal{Q} , $\bar{\Lambda}$, W , ρ , α are similar to the setting of TEMCP LRTC-Type-1. Within the framework of the ADMM, \mathcal{X} , \mathcal{Y} , $\bar{\Lambda}$, W , \mathcal{Q} are updated alternately in the order of $W \rightarrow \mathcal{Y} \rightarrow \bar{\Lambda} \rightarrow \mathcal{X} \rightarrow \mathcal{Q}$. The update equations are derived in the following.

Update W : Retaining only those components in $\mathcal{Y}_{l_1 l_2}$ in (34) that depend on $W_{l_1 l_2}$, we write

$$W_{l_1 l_2}^+ = \min_{W_{l_1 l_2}} \sum_{i_3=1}^{I_3} \|\bar{\mathcal{Y}}_{l_1 l_2}^{(i_3)}\|_{W_{l_1 l_2(:, i_3)}, * } + \frac{\gamma}{2} \|W_{l_1 l_2} - \bar{\Lambda}_{l_1 l_2}\|_F^2. \quad (35)$$

Algorithm 2 TEMCPTC-Type-1

Input: an incomplete tensor \mathcal{Z} , the index set of the known elements Ω , convergence criteria ϵ , maximum iteration number K .

Initialization: $\mathcal{X}^0 = \mathcal{Z}_{\Omega}$, $\mathcal{Y}_{l_1 l_2}^0 = \mathcal{X}^0$, $\rho_{l_1 l_2}^0 > 0$, $\mu > 1$.

while not converged and $k < K$ **do**

 Updating $\mathcal{Y}_{l_1 l_2}^k$ via (28);

 Updating $W_{l_1 l_2}^k$ via (30);

 Updating $\bar{\Lambda}_{l_1 l_2}^k$ via (31);

 Updating \mathcal{X}^k via (32);

 Updating the multipliers $\mathcal{Q}_{l_1 l_2}^k$ via (33);

$\rho_{l_1 l_2}^k = \mu \rho_{l_1 l_2}^{k-1}$, $k = k + 1$;

 Check the convergence conditions $\|\mathcal{X}^{k+1} - \mathcal{X}^k\|_{\infty} \leq \epsilon$.

end while

return \mathcal{X}^{k+1} .

Output: Completed tensor $\mathcal{X} = \mathcal{X}^{k+1}$.

Algorithm 3 TEMCPTC-Type-2

Input: an incomplete tensor \mathcal{Z} , the index set of the known elements Ω , convergence criteria ϵ , maximum iteration number K .

Initialization: $\mathcal{X}^0 = \mathcal{Z}_{\Omega}$, $\mathcal{Y}_{l_1 l_2}^0 = \mathcal{X}^0$, $\rho_{l_1 l_2}^0 > 0$, $\mu > 1$.

while not converged and $k < K$ **do**

 Updating $W_{l_1 l_2}^k$ via (36);

 Updating $\mathcal{Y}_{l_1 l_2}^k$ via (40);

 Updating $\bar{\Lambda}_{l_1 l_2}^k$ via (41);

 Updating \mathcal{X}^k via (42);

 Updating the multipliers $\mathcal{Q}_{l_1 l_2}^k$ via (43);

$\rho_{l_1 l_2}^k = \mu \rho_{l_1 l_2}^{k-1}$, $k = k + 1$;

 Check the convergence conditions $\|\mathcal{X}^{k+1} - \mathcal{X}^k\|_{\infty} \leq \epsilon$.

end while

return \mathcal{X}^{k+1} .

Output: Completed tensor $\mathcal{X} = \mathcal{X}^{k+1}$.

which has the following closed-form solution:

$$W_{l_1 l_2(:, i_3)}^+ = \max(\bar{\Lambda}_{l_1 l_2(:, i_3)} - \frac{\sigma(\bar{\mathcal{Y}}_{l_1 l_2}^{(i_3)})}{\gamma}, 0). \quad (36)$$

Update \mathcal{Y} : Fix other variables, and the corresponding optimization instructions are as follows:

$$\begin{aligned} \mathcal{Y}_{l_1 l_2}^+ = \min_{\mathcal{Y}_{l_1 l_2}} \quad & \alpha_{l_1 l_2} \sum_{i_3=1}^{I_3} \|\bar{\mathcal{Y}}_{l_1 l_2}^{(i_3)}\|_{W_{l_1 l_2(:, i_3)}, * } \\ & + \frac{\rho_{l_1 l_2}}{2} \|\mathcal{X} - \mathcal{Y}_{l_1 l_2} + \frac{\mathcal{Q}_{l_1 l_2}}{\rho_{l_1 l_2}}\|_F^2. \end{aligned} \quad (37)$$

To solve (37), we introduce the following theorem [41].

Theorem 10 (WTSVT Operator [41]): For any $\mathcal{Y} \in \mathbb{R}^{I_1 \times I_2 \times I_3}$ with t-SVD that $\mathcal{Y} = \mathcal{U} * \mathcal{S} * \mathcal{V}^H$, the WTSVT operator as

$$\mathcal{D}_{W, \tau}(\mathcal{Y}) = \mathcal{U} * \mathcal{S}_{W, \tau} * \mathcal{V}^H \quad (38)$$

where $W = (w_{ij})_{R \times I_3}$ and $\mathcal{S}_{W, \tau} = \text{ifft}((\bar{\mathcal{S}} - \tau \mathcal{W})_+, [], 3)$, in which $\mathcal{W} \in \mathbb{R}^{I_1 \times I_2 \times I_3}$ is f-diagonal whose diagonal entries

of the j th frontal slice are equal to the j th column of weight matrix W , and the WTSVT operator obeys

$$\mathcal{D}_{W, \tau}(\mathcal{Y}) = \arg \min_{\mathcal{X}} \tau \|\mathcal{X}\|_{W, *} + \frac{1}{2} \|\mathcal{X} - \mathcal{Y}\|_F^2 \quad (39)$$

if the weight matrix satisfies

$$0 \leq w_{1j} \leq w_{2j} \leq \dots \leq w_{mj}, j = 1, 2, \dots, I_3.$$

Theorem 10 is a natural extension of the tensor SVT [42]. So $\mathcal{Y}_{l_1 l_2}$ can be updated as

$$\mathcal{Y}_{l_1 l_2}^+ = \mathcal{D}_{W_{l_1 l_2}^+, \frac{\alpha_{l_1 l_2}}{\rho_{l_1 l_2}}}(\mathcal{X} + \frac{\mathcal{Q}_{l_1 l_2}}{\rho_{l_1 l_2}}).. \quad (40)$$

Update $\bar{\Lambda}$: The update for $\bar{\Lambda}_{l_1 l_2}$ turns out to be straightforward as the only term of $\mathcal{Y}_{l_1 l_2}$ in (34) that depends on $\bar{\Lambda}_{l_1 l_2}$ is a quadratic:

$$\bar{\Lambda}_{l_1 l_2}^+ = \min_{\bar{\Lambda}_{l_1 l_2}} \|W_{l_1 l_2} - \bar{\Lambda}_{l_1 l_2}\|_F^2 = W_{l_1 l_2}^+. \quad (41)$$

Update \mathcal{X} : The closed form of \mathcal{X} can be derived by setting the derivative of (34) with respect to zero. We can now update \mathcal{X} by the following equation:

$$\mathcal{X}^+ = \mathcal{P}_{\Omega^c} \left(\frac{\sum_{1 \leq l_1 < l_2 \leq N} \rho_{l_1 l_2} (\mathcal{Y}_{l_1 l_2} - \frac{\mathcal{Q}_{l_1 l_2}}{\rho_{l_1 l_2}})}{\sum_{1 \leq l_1 < l_2 \leq N} \rho_{l_1 l_2}} \right) + \mathcal{P}_{\Omega}(\mathcal{Z}) \quad (42)$$

Update \mathcal{Q} : Finally, multipliers $\mathcal{Q}_{l_1 l_2}$ are updated as follows:

$$\mathcal{Q}_{l_1 l_2}^+ = \mathcal{Q}_{l_1 l_2} + \rho_{l_1 l_2} (\mathcal{X} - \mathcal{Y}_{l_1 l_2}). \quad (43)$$

The optimization steps of TEMCPLRTC-Type-2 formulation are listed in Algorithm 3. It is not difficult to find that the contents of computation required by TEMCPTC-Type-1 and TEMCPTC-Type-2 iterations are basically the same, and the computational complexity of the two algorithms is the same. So we only need to discuss the computational complexity of one of the algorithms. The main per-iteration cost lies in the update of $\mathcal{Y}_{k_1 k_2}$, which requires computing t-SVD. The per-iteration complexity is $O(LE(\sum_{1 \leq k_1 < k_2 \leq N} [\log(le_{k_1 k_2}) + \min(I_{k_1}, I_{k_2})]))$, where $LE = \prod_{i=1}^N I_i$ and $le_{k_1 k_2} = LE / (I_{k_1} I_{k_2})$.

B. TEMCP TRPCA model

The optimization problem of TRPCA takes the following form:

$$\min_{\mathcal{L}, \mathcal{E}, \mathcal{N}} \sum_{1 \leq l_1 < l_2 \leq N} \|\mathcal{L}(l_1 l_2)\|_{\gamma, \bar{\Lambda}} + \tau_1 h_{\gamma, \bar{\Lambda}}(\mathcal{E}) + \tau_2 \|\mathcal{N}\|_F^2 \quad (44)$$

s.t. $\mathcal{T} = \mathcal{L} + \mathcal{E} + \mathcal{N},$

We solve the problem within the ADMM framework and rely on the proximal operators given in Theorem 8 and Theorem 9 to derive the optimization algorithms.

1) *Adaptive TEMCP TRPCA - Type-1:* An adaptive variant of the problem stated in (44) takes the following form:

$$\min_{\mathcal{L}, \mathcal{E}, \mathcal{N}, \mathcal{M}, \bar{\Lambda}, \bar{\lambda}, \mathcal{W}, \mathcal{Q}, \mathcal{G}} \sum_{1 \leq l_1 < l_2 \leq N} \beta_{l_1 l_2} \|\mathcal{M}_{l_1 l_2}(l_1 l_2)\|_{\gamma, \bar{\Lambda}_{l_1 l_2}} + \tau_1 h_{\gamma, \bar{\Lambda}}(\mathcal{E}) + \tau_2 \|\mathcal{N}\|_F^2 + \frac{\rho_{l_1 l_2}}{2} \|\mathcal{L} - \mathcal{M}_{l_1 l_2} + \frac{\mathcal{Q}_{l_1 l_2}}{\rho_{l_1 l_2}}\|_F^2 + \frac{\eta}{2} \|\mathcal{T} - (\mathcal{L} + \mathcal{E} + \mathcal{N}) + \frac{\mathcal{G}}{\eta}\|_F^2 \quad (45)$$

where \mathcal{M} and \mathcal{Q} are tensor sets; $\bar{\Lambda}$ and W are matrix sets; $\{\mathcal{M}_{l_1 l_2} = \mathcal{L}\}_{1 \leq l_1 < l_2 \leq N}^N$; $\{\mathcal{Q}\}_{1 \leq l_1 < l_2 \leq N}^N$, \mathcal{G} are Lagrangian multiplier; $\{\bar{\Lambda}\}_{1 \leq l_1 < l_2 \leq N}^N$, $\bar{\lambda}$ are MCP parameter and $\{W\}_{1 \leq l_1 < l_2 \leq N}^N$, \mathcal{W} are weights; $\{\rho_{l_1 l_2}\}_{1 \leq l_1 < l_2 \leq N}^N$, $\eta > 0$ are the augmented Lagrangian parameter; $\beta_{l_1 l_2} \geq 0$ are weights and $\sum_{1 \leq l_1 < l_2 \leq N} \beta_{l_1 l_2} = 1$; $\tau_1, \tau_2 > 0$.

Within the framework of the ADMM, \mathcal{L} , \mathcal{E} , \mathcal{N} , \mathcal{M} , $\bar{\Lambda}$, $\bar{\lambda}$, W , \mathcal{W} , \mathcal{Q} , \mathcal{G} are updated alternately in the order of $\mathcal{M} \rightarrow W \rightarrow \bar{\Lambda} \rightarrow \mathcal{L} \rightarrow \mathcal{N} \rightarrow \mathcal{E} \rightarrow \mathcal{W} \rightarrow \bar{\lambda} \rightarrow \mathcal{Q} \rightarrow \mathcal{G}$. The update equations are derived in the following.

Update \mathcal{M} : Fix other variables, and the corresponding optimization instructions are as follows:

$$\mathcal{M}_{l_1 l_2}^+ = \min_{\mathcal{M}_{l_1 l_2}} \beta_{l_1 l_2} \|\mathcal{M}_{l_1 l_2}(l_1 l_2)\|_{\gamma, \bar{\Lambda}_{l_1 l_2}} + \frac{\rho_{l_1 l_2}}{2} \|\mathcal{L} - \mathcal{M}_{l_1 l_2} + \frac{\mathcal{Q}_{l_1 l_2}}{\rho_{l_1 l_2}}\|_F^2.$$

Theorem 9 provides the following solution to the above problem:

$$\mathcal{M}_{l_1 l_2}^+ = S_{\gamma \rho_{l_1 l_2}, \frac{\bar{\Lambda}_{l_1 l_2} \rho_{l_1 l_2}}{\alpha_{l_1 l_2}, \alpha_{l_1 l_2}}}(\mathcal{L} + \frac{\mathcal{Q}_{l_1 l_2}}{\rho_{l_1 l_2}}). \quad (46)$$

where S denotes the proximal operator defined in (24).

Update W : Retaining only those components in $\mathcal{M}_{l_1 l_2}$ in (45) that depend on $W_{l_1 l_2}$, we write

$$W_{l_1 l_2}^+ = \min_{W_{l_1 l_2}} \sum_{i_3=1}^{I_3} \|\bar{\mathcal{M}}_{l_1 l_2}^{(i_3)}\|_{W_{l_1 l_2}(:, i_3), *} + \frac{\gamma}{2} \|W_{l_1 l_2} - \bar{\Lambda}_{l_1 l_2}\|_F^2. \quad (47)$$

which has the following closed-form solution:

$$W_{l_1 l_2}^{+}(:, i_3) = \max(\bar{\Lambda}_{l_1 l_2}(:, i_3) - \frac{\sigma(\mathcal{M}_{l_1 l_2}^{+(i_3)})}{\gamma}, 0). \quad (48)$$

Update $\bar{\Lambda}$: The update for $\bar{\Lambda}_{l_1 l_2}$ turns out to be straightforward as the only term of $\mathcal{M}_{l_1 l_2}$ in (45) that depends on $\bar{\Lambda}_{l_1 l_2}$ is a quadratic:

$$\bar{\Lambda}_{l_1 l_2}^+ = \min_{\bar{\Lambda}_{l_1 l_2}} \|W_{l_1 l_2} - \bar{\Lambda}_{l_1 l_2}\|_F^2 = W_{l_1 l_2}^+. \quad (49)$$

Update \mathcal{L} : The closed form of \mathcal{L} can be derived by setting the derivative of (45) with respect to zero. We can now update \mathcal{L} by the following equation:

$$\mathcal{L}^+ = \frac{\sum_{1 \leq l_1 < l_2 \leq N} \rho_{l_1 l_2} (\mathcal{M}_{l_1 l_2} - \frac{\mathcal{Q}_{l_1 l_2}}{\rho_{l_1 l_2}}) + \eta(\mathcal{T} - \mathcal{N} - \mathcal{E} + \frac{\mathcal{G}}{\eta})}{\sum_{1 \leq l_1 < l_2 \leq N} \rho_{l_1 l_2} + \eta} \quad (50)$$

Update \mathcal{N} : We update \mathcal{N} by the following equation:

$$\mathcal{L}^+ = \frac{\eta \mathcal{T} - \eta \mathcal{L} - \eta \mathcal{E} + \mathcal{G}}{2\tau_2 + \eta} \quad (51)$$

Update \mathcal{E} : Fix other variables, and the corresponding optimization instructions are as follows:

$$\mathcal{E}^+ = \min_{\mathcal{E}} \tau_1 h_{\gamma, \bar{\lambda}}(\mathcal{E}) + \frac{\eta}{2} \|\mathcal{T} - (\mathcal{L} + \mathcal{E} + \mathcal{N}) + \frac{\mathcal{G}}{\eta}\|_F^2.$$

Theorem 8 provides the following solution to the above problem:

$$\mathcal{E}_{l_1 l_2}^+ = S_{\frac{\gamma \eta}{\tau_1}, \frac{\bar{\lambda} \eta}{\tau_1}}(\mathcal{T} - \mathcal{L} - \mathcal{N} + \frac{\mathcal{G}}{\eta}). \quad (52)$$

where S denotes the proximal operator defined in (22).

Update \mathcal{W} : Retaining only those components in \mathcal{E} in (45) that depend on \mathcal{W} , we write

$$\mathcal{W}^+ = \min_{\mathcal{W}} \|\mathcal{E}\|_{\mathcal{W}, 1} + \frac{\gamma}{2} \|\mathcal{W} - \bar{\lambda}\|_F^2. \quad (53)$$

This is an l_1 optimization problem and the solution is given by the element-wise soft-threshold operation:

$$\mathcal{W}^+ = \max(\bar{\lambda} - \frac{|\mathcal{E}|}{\gamma}, 0). \quad (54)$$

Update $\bar{\lambda}$: The update for $\bar{\lambda}$ turns out to be straightforward as the only term of \mathcal{M} in (45) that depends on $\bar{\lambda}$ is a quadratic:

$$\bar{\lambda}_{l_1 l_2}^+ = \min_{\bar{\lambda}_{l_1 l_2}} \|W_{l_1 l_2} - \bar{\lambda}_{l_1 l_2}\|_F^2 = \mathcal{W}_{l_1 l_2}^+. \quad (55)$$

Update \mathcal{Q}, \mathcal{G} : Finally, multipliers $\mathcal{Q}_{l_1 l_2}, \mathcal{G}$ are updated as follows:

$$\mathcal{Q}_{l_1 l_2}^+ = \mathcal{Q}_{l_1 l_2} + \rho_{l_1 l_2} (\mathcal{L} - \mathcal{M}_{l_1 l_2}). \quad (56)$$

$$\mathcal{G}^+ = \mathcal{G} + \eta (\mathcal{T} - (\mathcal{L} + \mathcal{E} + \mathcal{N})). \quad (57)$$

The optimization steps of TEMCPTRPCA-Type-1 formulation are listed in Algorithm 4.

Algorithm 4 TEMCPTRPCA-Type-1

Input: The corrupted observation tensor \mathcal{T} , convergence criteria ϵ , maximum iteration number K .

Initialization: $\mathcal{L}^0 = \mathcal{T}$, $\mathcal{M}_{l_1 l_2}^0 = \mathcal{L}^0$, $\rho_{l_1 l_2}^0 > 0$, $\eta > 0$, $\mu > 1$.

while not converged and $k < K$ **do**

 Updating $\mathcal{M}_{l_1 l_2}^k$ via (46);

 Updating $W_{l_1 l_2}^k$ via (48);

 Updating $\bar{\Lambda}_{l_1 l_2}^k$ via (49);

 Updating \mathcal{L}^k via (50);

 Updating \mathcal{N}^k via (51);

 Updating \mathcal{E}^k via (52);

 Updating \mathcal{W}^k via (54);

 Updating $\bar{\lambda}^k$ via (55);

 Updating the multipliers $\mathcal{Q}_{l_1 l_2}^k$ via (56);

 Updating \mathcal{G}^k via (57);

$\rho_{l_1 l_2}^k = \mu \rho_{l_1 l_2}^{k-1}$, $\eta^k = \mu \eta^{k-1}$, $k = k + 1$;

 Check the convergence conditions $\|\mathcal{L}^{k+1} - \mathcal{L}^k\|_{\infty} \leq \epsilon$.

end while

return \mathcal{L}^{k+1} and \mathcal{E}^{k+1} .

Output: \mathcal{L} and \mathcal{E} .

Algorithm 5 TEMCPTRPCA-Type-2

Input: The corrupted observation tensor \mathcal{T} , convergence criteria ϵ , maximum iteration number K .

Initialization: $\mathcal{L}^0 = \mathcal{T}$, $\mathcal{M}_{l_1 l_2}^0 = \mathcal{L}^0$, $\rho_{l_1 l_2}^0 > 0$, $\eta > 0$, $\mu > 1$.

while not converged and $k < K$ **do**

 Updating $W_{l_1 l_2}^k$ via (60);

 Updating $\mathcal{M}_{l_1 l_2}^k$ via (62);

 Updating \mathcal{L}^k via (64);

 Updating $\bar{\Lambda}_{l_1 l_2}^k$ via (63);

 Updating \mathcal{N}^k via (65);

 Updating \mathcal{W}^k via (67);

 Updating \mathcal{E}^k via (69);

 Updating $\bar{\lambda}^k$ via (70);

 Updating the multipliers $\mathcal{Q}_{l_1 l_2}^k$ via (71);

 Updating \mathcal{G}^k via (72);

$\rho_{l_1 l_2}^k = \mu \rho_{l_1 l_2}^{k-1}$, $\eta^k = \mu \eta^{k-1}$, $k = k + 1$;

 Check the convergence conditions $\|\mathcal{L}^{k+1} - \mathcal{L}^k\|_{\infty} \leq \epsilon$.

end while

return \mathcal{L}^{k+1} and \mathcal{E}^{k+1} .

Output: \mathcal{L} and \mathcal{E} .

2) *Adaptive TEMCP TRPCA - Type-2:* Another adaptive variant of the problem stated in (44) takes the following form:

$$\begin{aligned} \min_{\mathcal{L}, \mathcal{E}, \mathcal{N}, \mathcal{M}, \bar{\Lambda}, \bar{\lambda}, \mathcal{W}, \mathcal{Q}, \mathcal{G}} \sum_{1 \leq l_1 < l_2 \leq N} \beta_{l_1 l_2} \sum_{i_3=1}^{I_3} \|\bar{\mathcal{M}}_{l_1 l_2}^{(i_3)}\|_{W_{l_1 l_2(:, i_3)}, *}, \\ + \frac{\gamma}{2} \|W_{l_1 l_2} - \bar{\Lambda}_{l_1 l_2}\|_F^2 + \tau_1 (\|\mathcal{E}\|_{\mathcal{W}, 1} + \frac{\gamma}{2} \|\mathcal{W} - \bar{\lambda}\|_F^2) \\ + \tau_2 \|\mathcal{N}\|_F^2 + \frac{\rho_{l_1 l_2}}{2} \|\mathcal{L} - \mathcal{M}_{l_1 l_2} + \frac{\mathcal{Q}_{l_1 l_2}}{\rho_{l_1 l_2}}\|_F^2 \\ + \frac{\eta}{2} \|\mathcal{T} - (\mathcal{L} + \mathcal{E} + \mathcal{N}) + \frac{\mathcal{G}}{\eta}\|_F^2 \end{aligned} \quad (58)$$

where $\mathcal{M}, \mathcal{Q}, \mathcal{G}, \bar{\Lambda}, W, \bar{\lambda}, \mathcal{W}, \rho, \eta, \beta, \tau_1, \tau_2$ are similar to the setting of TEMCP TRPCA-Type-1. Within the framework of the ADMM, $\mathcal{L}, \mathcal{E}, \mathcal{N}, \mathcal{M}, \bar{\Lambda}, \bar{\lambda}, W, \mathcal{W}, \mathcal{Q}, \mathcal{G}$ are updated alternately in the order of $W \rightarrow \mathcal{M} \rightarrow \bar{\Lambda} \rightarrow \mathcal{L} \rightarrow \mathcal{N} \rightarrow \mathcal{W} \rightarrow \mathcal{E} \rightarrow \bar{\lambda} \rightarrow \mathcal{Q} \rightarrow \mathcal{G}$. The update equations are derived in the following.

Update W : Retaining only those components in $\mathcal{M}_{l_1 l_2}$ in (45) that depend on $W_{l_1 l_2}$, we write

$$W_{l_1 l_2}^+ = \min_{W_{l_1 l_2}} \sum_{i_3=1}^{I_3} \|\bar{\mathcal{M}}_{l_1 l_2}^{(i_3)}\|_{W_{l_1 l_2(:, i_3)}, *} + \frac{\gamma}{2} \|W_{l_1 l_2} - \bar{\Lambda}_{l_1 l_2}\|_F^2. \quad (59)$$

which has the following closed-form solution:

$$W_{l_1 l_2(:, i_3)}^+ = \max(\bar{\Lambda}_{l_1 l_2(:, i_3)} - \frac{\sigma(\mathcal{M}_{l_1 l_2}^{(i_3)})}{\gamma}, 0). \quad (60)$$

Update \mathcal{M} : Fix other variables, and the corresponding optimization instructions are as follows:

$$\begin{aligned} \mathcal{M}_{l_1 l_2}^+ = \min_{\mathcal{M}_{l_1 l_2}} \beta_{l_1 l_2} \sum_{i_3=1}^{I_3} \|\bar{\mathcal{M}}_{l_1 l_2}^{(i_3)}\|_{W_{l_1 l_2(:, i_3)}, *} \\ + \frac{\rho_{l_1 l_2}}{2} \|\mathcal{L} - \mathcal{M}_{l_1 l_2} + \frac{\mathcal{Q}_{l_1 l_2}}{\rho_{l_1 l_2}}\|_F^2. \end{aligned} \quad (61)$$

Similar to the solution in TEMCPTC-Type-2, the problem is solved as follows:

$$\mathcal{M}_{l_1 l_2}^+ = \mathcal{D}_{W_{l_1 l_2}^+, \beta_{l_1 l_2}, \rho_{l_1 l_2}}(\mathcal{L} + \frac{Q_{l_1 l_2}}{\rho_{l_1 l_2}}).. \quad (62)$$

Update $\bar{\Lambda}$: The update for $\bar{\Lambda}_{l_1 l_2}$ turns out to be straightforward as the only term of $\mathcal{M}_{l_1 l_2}$ in (58) that depends on $\bar{\Lambda}_{l_1 l_2}$ is a quadratic:

$$\bar{\Lambda}_{l_1 l_2}^+ = \min_{\bar{\Lambda}_{l_1 l_2}} \|W_{l_1 l_2} - \bar{\Lambda}_{l_1 l_2}\|_F^2 = W_{l_1 l_2}^+. \quad (63)$$

Update \mathcal{L} : The closed form of \mathcal{L} can be derived by setting the derivative of (45) with respect to zero. We can now update \mathcal{L} by the following equation:

$$\mathcal{L}^+ = \frac{\sum_{1 \leq l_1 < l_2 \leq N} \rho_{l_1 l_2} (\mathcal{M}_{l_1 l_2} - \frac{Q_{l_1 l_2}}{\rho_{l_1 l_2}}) + \eta(\mathcal{T} - \mathcal{N} - \mathcal{E} + \frac{\mathcal{G}}{\eta})}{\sum_{1 \leq l_1 < l_2 \leq N} \rho_{l_1 l_2} + \eta} \quad (64)$$

Update \mathcal{N} : We update \mathcal{N} by the following equation:

$$\mathcal{N}^+ = \frac{\eta\mathcal{T} - \eta\mathcal{L} - \eta\mathcal{E} + \mathcal{G}}{2\tau_2 + \eta} \quad (65)$$

Update \mathcal{W} : Retaining only those components in \mathcal{E} in (45) that depend on \mathcal{W} , we write

$$\mathcal{W}^+ = \min_{\mathcal{W}} \|\mathcal{E}\|_{\mathcal{W}, 1} + \frac{\gamma}{2} \|\mathcal{W} - \bar{\lambda}\|_F^2. \quad (66)$$

This is an l_1 optimization problem and the solution is given by the element-wise soft-threshold operation:

$$\mathcal{W}^+ = \max(\bar{\lambda} - \frac{|\mathcal{E}|}{\gamma}, 0). \quad (67)$$

Update \mathcal{E} : Fix other variables, and the corresponding optimization instructions are as follows:

$$\mathcal{E}^+ = \min_{\mathcal{E}} \tau_1 \|\mathcal{E}\|_{\mathcal{W}, 1} + \frac{\eta}{2} \|\mathcal{T} - (\mathcal{L} + \mathcal{E} + \mathcal{N}) + \frac{\mathcal{G}}{\eta}\|_F^2.$$

The optimization of the problem involves weighted l_1 norm whose solution can be given by a soft-thresholding for each element.

$$\mathcal{E}_{l_1 l_2}^+ = \max\{\mathcal{T} - \mathcal{L} - \mathcal{N} + \frac{\mathcal{G}}{\eta} \mid -\frac{\mathcal{W}}{\eta}, 0\} \quad (68)$$

$$\odot \text{sign}(\mathcal{T} - \mathcal{L} - \mathcal{N} + \frac{\mathcal{G}}{\eta}). \quad (69)$$

Update $\bar{\lambda}$: The update for $\bar{\lambda}$ turns out to be straightforward as the only term of \mathcal{M} in (58) that depends on $\bar{\lambda}$ is a quadratic:

$$\bar{\lambda}_{l_1 l_2}^+ = \min_{\bar{\lambda}_{l_1 l_2}} \|W_{l_1 l_2} - \bar{\lambda}_{l_1 l_2}\|_F^2 = \mathcal{W}_{l_1 l_2}^+. \quad (70)$$

Update Q, \mathcal{G} : Finally, multipliers $Q_{l_1 l_2}, \mathcal{G}$ are updated as follows:

$$Q_{l_1 l_2}^+ = Q_{l_1 l_2} + \rho_{l_1 l_2} (\mathcal{L} - \mathcal{M}_{l_1 l_2}). \quad (71)$$

$$\mathcal{G}^+ = \mathcal{G} + \eta(\mathcal{T} - (\mathcal{L} + \mathcal{E} + \mathcal{N})). \quad (72)$$

The optimization steps of TEMCPTRPCA-Type-2 formulation are listed in Algorithm 5. Similar to low-rank tensor completeness, the algorithm for tensor robust principal component analysis only needs to study the complexity of one algorithm. The main per-iteration cost lies in the update of $\mathcal{M}_{l_1 l_2}$, which requires computing t-SVD. The per-iteration complexity is $O(LE(\sum_{1 \leq l_1 < l_2 \leq N} [\log(le_{l_1 l_2}) + \min(I_{l_1}, I_{l_2})]))$, where $LE = \prod_{i=1}^N I_i$ and $le_{l_1 l_2} = LE / (I_{l_1} I_{l_2})$.

TABLE I
THE NAMES AND CORRESPONDING LABELS OF INDIVIDUAL MSI IN THE DATABASE CAVE.

ID	MSI name	ID	MSI name
1	watercolors	17	fake_and_real_tomatoes
2	thread_spools	18	fake_and_real_sushi
3	superballs	19	fake_and_real_strawberries
4	stuffed_toys	20	fake_and_real_peppers
5	sponges	21	fake_and_real_lemons
6	real_and_fake_peppers	22	fake_and_real_lemon_slices
7	real_and_fake_apples	23	fake_and_real_food
8	pompoms	24	fake_and_real_beers
9	photo_and_face	25	face
10	paints	26	egyptian_statue
11	oil_painting	27	cloth
12	jelly_beans	28	clay
13	hairs	29	chart_and_stuffed_toy
14	glass_tiles	30	beads
15	flowers	31	balloons
16	feathers	32	cd

VI. EXPERIMENTS

We evaluate the performance of the proposed FFM-based LRTC and TRPCA methods. Both real-world data are tested. We employ the peak signal-to-noise rate (PSNR), the structural similarity (SSIM) [43], the feature similarity (FSIM) [44], and erreur relative globale adimensionnelle de synthèse (ERGAS) [45] to measure the quality of the recovered results. PSNR, SSIM and FSIM are the bigger the better, and the ERGAS is the smaller the better. For simplicity, TEMCPTC-Type-1 and TEMCPTRPCA-Type-1 are denoted as TEMCP1, and similarly, TEMCPTC-Type-2 and TEMCPTRPCA Type-2 are denoted as TEMCP2. All tests are implemented on the Windows 10 platform and MATLAB (R2019a) with an Intel Core i7-10875H 2.30 GHz and 32 GB of RAM.

A. Low-rank tensor completion

In this section, we test four kinds of real-world data: MSI, MRI and CV. The methodology for sampling the data is purely random sampling. The compared LRTC methods are as follows: HaLRTC [46], LRTCTV-I [47] representing the state of the art for the Tucker-decomposition-based method; and TNN [42], PSTNN [49], FTNN [50], WSTNN [27] representing the state of the art for the t-SVD-based method; and minmax concave plus penalty-based TC method (McpTC) [52] and a novel low-rank tensor completion model using smooth matrix factorization (SMFLRTC)[53]. Because the TNN, the PSTNN, the FTNN, and the SMFLRTC apply only to three-order tensors, in all four-order tensor tests, we first reshape the four-order tensor into three-order tensors and then test the performances of these methods.

1) *MSI completion:* We test 32 MSIs in the dataset CAVE¹. All testing data are of size $256 \times 256 \times 31$. First, we labeled 32 MSIs in the database. The MSI names and their corresponding labels are listed in Table I. Then, we randomly selected six from 32 MSI, brings the different sampling rate and different band visual results shown in Fig.2. The individual MSI names and their corresponding bands are written out

¹<http://www.cs.columbia.edu/CAVE/databases/multispectral/>

TABLE II
THE AVERAGE PSNR, SSIM, FSIM AND ERGAS VALUES FOR 32 MSIS TESTED BY OBSERVED AND THE TWELVE UTILIZED LRTC METHODS.

SR	5%				10%				20%				Time(s)
	Method	PSNR	SSIM	FSIM	ERGAS	PSNR	SSIM	FSIM	ERGAS	PSNR	SSIM	FSIM	
Observed	15.438	0.153	0.644	845.344	15.672	0.194	0.646	822.816	16.185	0.269	0.651	775.705	0.000
HaLRTC	25.370	0.774	0.838	298.223	29.843	0.856	0.894	185.272	35.030	0.929	0.946	105.307	10.320
TNN	25.334	0.713	0.817	289.753	33.128	0.880	0.918	127.850	40.227	0.964	0.972	58.756	30.438
LRTC-TV-I	25.905	0.800	0.835	276.199	30.711	0.890	0.906	162.807	35.525	0.949	0.957	94.165	181.906
McpTC	32.438	0.875	0.909	133.545	35.940	0.924	0.943	92.308	40.541	0.964	0.972	55.941	184.511
PSTNN	18.712	0.474	0.650	574.715	23.211	0.683	0.783	353.014	34.298	0.924	0.941	116.606	32.488
SMFLRTC	31.511	0.888	0.918	145.396	39.054	0.964	0.971	61.936	44.029	0.981	0.985	37.622	519.829
FTNN	32.578	0.899	0.923	132.186	37.176	0.954	0.963	78.911	43.064	0.984	0.987	41.437	183.908
WSTNN	31.398	0.806	0.911	209.435	40.109	0.981	0.981	53.190	47.111	0.995	0.995	24.817	47.069
TEMCP1	37.558	0.960	0.961	69.608	43.555	0.988	0.988	35.633	50.976	0.997	0.997	15.951	92.761
TEMCP2	37.594	0.958	0.960	69.693	43.503	0.988	0.988	35.870	50.317	0.997	0.997	17.093	102.855



Fig. 2. (a) Original image. (b) Observed image. (c) HaLRTC. (d) TNN. (e) LRTC-TV-I. (f) McpTC. (g) PSTNN. (h) SMFLRTC. (i) FTNN. (j) WSTNN. (k) TEMCP1. (l) TEMCP2. SR: top 2 rows is 5%, middle 2 rows is 10% and last 2 rows is 20%. The rows of MSIs are in order: pompoms, fake_and_real_sushi, watercolors, clay, chart_and_stuffed_toy, fake_and_real_beers. The corresponding bands in each row are: 14, 4, 9, 21, 30, 13.

in the caption to Fig.2. As can be seen from the figure, the visual effects of TEMCP1 and TEMCP2 are superior to those of the comparison method under no circumstances, and the effects obtained by the two algorithms are basically consistent, which is consistent with our theory. To further highlight the superiority of our method, the average quantitative results of 32 MSI are listed in Table II. The results in the table show that the PSNR of the two complete algorithms proposed by us is 3dB higher than that of the suboptimal method when the sampling rate is 10% and 20%, and even reaches 5dB when the sampling rate is 5%. It is not difficult to find that TEMCP1 and TEMCP2 are obviously superior to McpTC method which also adopts MCP non-convex penalty function, which indicates that the adaptive method proposed by us is superior to MCP

function directly. More experimental results are available in the appendix.

2) *MRI completion*: We test the performance of the proposed method and the comparison method on MRI² data with the size of $181 \times 217 \times 181$. First of all, we show the restored visual effects of MRI data at 5%, 10% and 20% sampling rates in Fig.3. Our method is clearly superior to the comparative method. Then, we listed in Table III the average quantitative results of frontal sections of MRI restored by all methods at different sampling rates. Obviously, the PSNR of our method is at least 0.6dB higher than that of the suboptimal method, and SSIM, FSIM and ERGAS are significantly better than that

²http://brainweb.bic.mni.mcgill.ca/brainweb/selection_normal.html

TABLE III
THE PSNR, SSIM, FSIM AND ERGAS VALUES OUTPUT BY BY OBSERVED AND THE TWELVE UTILIZED LRTC METHODS FOR MRI.

SR	5%				10%				20%				Time(s)
Method	PSNR	SSIM	FSIM	ERGAS	PSNR	SSIM	FSIM	ERGAS	PSNR	SSIM	FSIM	ERGAS	
Observed	11.399	0.310	0.530	1021.187	11.633	0.323	0.565	993.935	12.145	0.350	0.612	937.066	0.000
HaLRTC	17.282	0.297	0.636	538.383	20.114	0.439	0.725	390.915	24.449	0.659	0.829	235.279	21.061
TNN	22.710	0.472	0.743	303.286	26.058	0.643	0.812	205.896	29.950	0.798	0.881	131.536	89.715
LRTCTV-I	19.381	0.597	0.702	432.473	22.850	0.749	0.805	294.467	28.205	0.890	0.908	155.781	499.953
McpTC	28.178	0.756	0.846	149.290	31.407	0.843	0.887	103.161	35.548	0.937	0.941	64.066	516.453
PSTNN	16.141	0.196	0.589	609.873	22.431	0.438	0.723	308.514	29.564	0.766	0.870	137.890	103.374
SMFLRTC	28.546	0.795	0.860	146.226	32.265	0.900	0.914	94.134	35.045	0.943	0.942	67.542	1569.508
FTNN	24.817	0.689	0.835	233.015	28.287	0.826	0.895	152.966	32.683	0.922	0.945	90.357	1184.841
WSTNN	25.535	0.708	0.825	211.561	29.032	0.837	0.887	139.492	33.429	0.927	0.940	83.626	235.504
TEMCP1	29.319	0.810	0.875	132.208	32.993	0.900	0.922	86.727	37.077	0.958	0.960	53.749	488.162
TEMCP2	29.565	0.821	0.880	128.514	33.266	0.910	0.926	84.339	36.963	0.959	0.960	54.648	540.822

TABLE IV
THE AVERAGE PSNR, SSIM, FSIM AND ERGAS VALUES FOR 7 CVs TESTED BY OBSERVED AND THE TWELVE UTILIZED LRTC METHODS.

SR	5%				10%				20%				Time(s)
Method	PSNR	SSIM	FSIM	ERGAS	PSNR	SSIM	FSIM	ERGAS	PSNR	SSIM	FSIM	ERGAS	
Observed	5.793	0.011	0.420	1194.927	6.027	0.019	0.423	1163.111	6.539	0.034	0.429	1096.563	0.000
HaLRTC	17.338	0.488	0.696	329.535	21.112	0.621	0.773	215.395	24.969	0.772	0.862	137.789	16.120
TNN	27.065	0.772	0.886	113.252	30.445	0.855	0.928	79.569	33.671	0.910	0.955	56.765	45.987
LRTCTV-I	19.487	0.579	0.692	273.309	21.207	0.655	0.771	228.406	25.774	0.816	0.881	127.392	325.894
McpTC	23.358	0.660	0.816	168.536	28.066	0.814	0.898	97.323	30.887	0.882	0.934	70.135	352.237
PSTNN	16.151	0.312	0.665	365.048	27.874	0.777	0.889	103.146	33.246	0.906	0.952	58.860	46.545
SMFLRTC	26.072	0.777	0.873	120.030	31.830	0.906	0.949	63.817	35.512	0.946	0.971	42.867	1542.486
FTNN	25.317	0.766	0.871	137.283	28.550	0.858	0.918	93.375	32.213	0.924	0.954	61.397	406.923
WSTNN	29.233	0.872	0.920	88.331	32.646	0.923	0.952	62.033	36.543	0.960	0.975	40.856	219.348
TEMCP1	30.497	0.883	0.934	76.802	34.350	0.937	0.962	51.623	38.303	0.968	0.981	33.437	286.120
TEMCP2	30.849	0.890	0.938	73.939	34.639	0.939	0.964	50.115	38.416	0.968	0.981	32.986	315.575

of the suboptimal method.

3) *CV completion*: We test seven CVs³(respectively named news, akiyo, foreman, hall, highway, container, coastguard) of size $144 \times 176 \times 3 \times 50$. Firstly, we show the visual results of 7 CVs in our experiment in Fig. 4, in which the frame number and sampling rate corresponding to each CV are described in the caption in the figure. It is not hard to see from the picture, the recovery of our method on the vision effect is better. Furthermore, we listed the average quantitative results of 7 CV in Table IV. At this time, the suboptimal method is WSTNN. When the sampling rate is 5%, the PSNR of our method is 1.2dB higher than it, and even nearly exceeds 2dB when the sampling rate is 20%.

B. Tensor robust principal component analysis

In this section, we evaluate the performance of the proposed FFM-based TRPCA method by HSI denoising. The compared TRPCA methods include the SNN [54], TNN [37], 3DTNN and 3DLogTNN [51].

1) *HSI denoising*: We test the Pavia University and Washington DC Mall data sets, where Pavia data size is $200 \times 200 \times 80$ and Washington DC Mall data size is $256 \times 256 \times 150$. We divided the mixed noise into two kinds, one is independent identically distributed Gaussian noise plus independent identically distributed pepper and salt noise, the other is non i.i.d. Gaussian noise plus i.i.d pepper and salt noise. In Table V and VI, we list the quantitative numerical results

of Pavia University and Washington DC Mall Data under 6 combinations of these two kinds of noise respectively. It can be seen that even under the influence of the most serious noise, the PSNR of the obtained results is still 0.4 dB higher than that of the suboptimal method 3DLogTNN, and the improved effect becomes more obvious with the reduction of noise. In Fig.5, we show the visual results of the two kinds of data in sequence according to the noise order in Table V and VI. The corresponding spectral band number is: 30, 40, 20, 130, 25, 50. It is easy to know from the figure that our method has better denoising effect compared with the comparison method.

C. Convergency Behaviours

We take the completeness of MRI, CV, MSI data and the robust principal component analysis of HSI as examples to illustrate the convergence behavior of the algorithm under different sampling rates and different mixed noise. We have drawn $\|\mathcal{X}^{k+1} - \mathcal{X}^k\|_\infty$ and $\|\mathcal{L}^{k+1} - \mathcal{L}^k\|_\infty$ for each iteration in the figure 6. It can be seen that our algorithm converges stably, and the convergence speed is also very fast.

VII. CONCLUSION

In this paper, a new method called tensor equivalent Minimax-Concave Penalty is proposed to transform the constant parameters in Minimax-Concave Penalty functions into reasonable variables, which enable it to realize adaptive update in the algorithm. Compared with Minimax-Concave Penalty

³<http://trace.eas.asu.edu/yuv/>

TABLE V

THE PSNR, SSIM, FSIM AND ERGAS VALUES OUTPUT BY BY OBSERVED AND THE SIX UTILIZED TRPCA METHODS FOR PAVIA CITY CENTER.

Mixed noise		Noise	SNN	TNN	3DTNN	3DLogTNN	TEMCP1	TEMCP2
$\sigma = 0.1 \nu = 0.2$	PSNR	11.189	24.282	22.647	31.925	32.874	34.228	34.192
	SSIM	0.104	0.631	0.527	0.927	0.937	0.945	0.945
	FSIM	0.493	0.788	0.778	0.952	0.956	0.962	0.962
	ERGAS	923.439	202.894	245.224	84.641	77.155	65.864	66.352
$\sigma = 0.1 \nu = 0.3$	PSNR	9.630	23.568	21.206	30.831	32.907	33.252	33.185
	SSIM	0.066	0.579	0.446	0.905	0.933	0.933	0.933
	FSIM	0.437	0.763	0.741	0.939	0.954	0.955	0.954
	ERGAS	1105.166	220.475	289.340	95.738	76.052	73.336	74.280
$\sigma = 0.2 \nu = 0.2$	PSNR	9.754	21.963	17.411	27.804	29.195	30.455	30.195
	SSIM	0.072	0.433	0.256	0.824	0.852	0.887	0.884
	FSIM	0.425	0.690	0.632	0.893	0.914	0.921	0.919
	ERGAS	1087.468	265.871	448.380	134.893	115.236	101.132	104.091
$\sigma = 0.2 \nu = 0.3$	PSNR	8.572	21.605	16.214	25.649	20.864	29.081	29.180
	SSIM	0.050	0.394	0.202	0.715	0.423	0.863	0.865
	FSIM	0.391	0.667	0.598	0.852	0.734	0.911	0.910
	ERGAS	1246.778	277.303	514.939	172.916	300.411	118.334	116.844
σ follows U(0.05-0.15) $\nu = 0.2$	PSNR	11.241	24.757	23.512	32.506	34.310	34.766	34.854
	SSIM	0.107	0.663	0.574	0.935	0.951	0.952	0.952
	FSIM	0.498	0.805	0.798	0.957	0.966	0.967	0.967
	ERGAS	920.091	192.576	224.689	80.020	65.633	62.395	62.221
σ follows U(0.1-0.2) $\nu = 0.2$	PSNR	10.492	22.879	19.692	29.591	31.533	32.040	31.970
	SSIM	0.087	0.518	0.367	0.879	0.913	0.914	0.910
	FSIM	0.457	0.733	0.698	0.923	0.943	0.941	0.941
	ERGAS	1001.324	239.144	345.491	110.397	88.812	84.065	84.350
	TIME(s)	0.000	13.856	29.230	54.109	70.040	89.961	88.537

TABLE VI

THE PSNR, SSIM, FSIM AND ERGAS VALUES OUTPUT BY BY OBSERVED AND THE SIX UTILIZED TRPCA METHODS FOR WASHINGTON DC.

Mixed noise		Noise	SNN	TNN	3DTNN	3DLogTNN	TEMCP1	TEMCP2
$\sigma = 0.1 \nu = 0.2$	PSNR	10.863	25.322	22.879	31.360	34.967	35.486	35.540
	SSIM	0.102	0.671	0.511	0.871	0.950	0.949	0.949
	FSIM	0.476	0.821	0.768	0.937	0.969	0.970	0.970
	ERGAS	1106.333	209.180	272.561	101.837	68.035	64.026	63.634
$\sigma = 0.1 \nu = 0.3$	PSNR	9.286	24.577	21.508	28.255	34.004	34.697	34.764
	SSIM	0.065	0.630	0.438	0.758	0.939	0.941	0.941
	FSIM	0.422	0.798	0.733	0.889	0.963	0.965	0.965
	ERGAS	1327.142	228.451	319.008	145.507	76.018	70.089	69.559
$\sigma = 0.2 \nu = 0.2$	PSNR	9.502	23.015	17.358	24.339	30.308	30.910	31.195
	SSIM	0.072	0.519	0.250	0.567	0.886	0.879	0.888
	FSIM	0.409	0.737	0.614	0.807	0.939	0.936	0.936
	ERGAS	1289.724	274.011	516.603	229.256	116.129	108.751	104.987
$\sigma = 0.2 \nu = 0.3$	PSNR	8.300	22.523	16.052	21.534	19.808	29.007	29.340
	SSIM	0.050	0.485	0.197	0.419	0.358	0.853	0.862
	FSIM	0.377	0.715	0.578	0.740	0.694	0.926	0.925
	ERGAS	1482.771	290.546	601.136	318.099	389.882	135.236	129.840
σ follows U(0.05-0.15) $\nu = 0.2$	PSNR	10.819	25.439	23.148	31.304	35.120	35.722	35.850
	SSIM	0.102	0.678	0.524	0.863	0.953	0.953	0.953
	FSIM	0.476	0.825	0.775	0.933	0.970	0.972	0.972
	ERGAS	1112.822	207.267	266.091	106.598	67.020	62.200	61.357
σ follows U(0.1-0.2) $\nu = 0.2$	PSNR	10.227	24.012	19.898	27.392	32.510	33.326	33.247
	SSIM	0.087	0.589	0.362	0.720	0.922	0.921	0.922
	FSIM	0.441	0.777	0.687	0.872	0.954	0.954	0.954
	ERGAS	1191.208	244.086	386.355	166.419	90.662	82.400	83.048
	TIME(s)	0.000	44.597	95.571	196.570	293.184	326.818	321.230

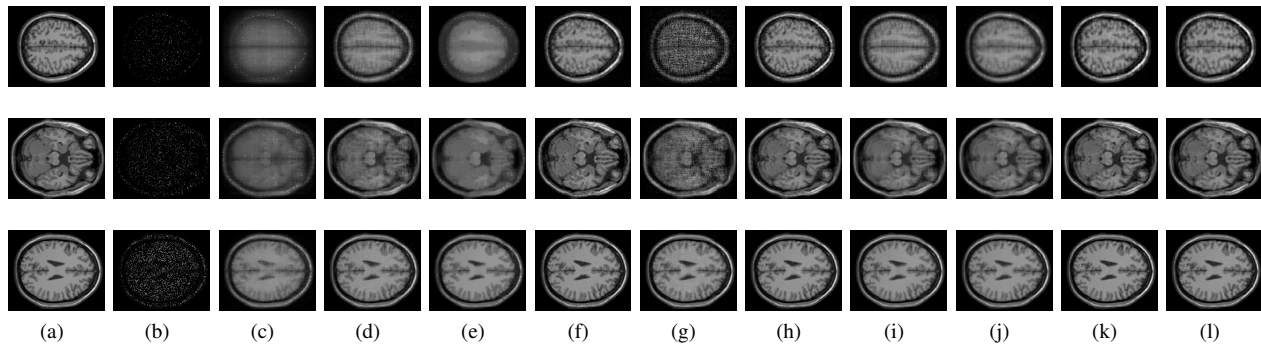


Fig. 3. (a) Original image. (b) Observed image. (c) HaLRTC. (d) TNN. (e) LRTC-TV-I. (f) McpTC. (g) PSTNN. (h) SMFLRTC. (i) FTNN. (j) WSTNN. (k) TEMCP1. (l) TEMCP2. Each type of slice: the first row is the 120th slice with a sampling rate of 5%, the second row is the 50th slice with a sampling rate of 10%, and the third row is the 100th slice with a sampling rate of 20%.

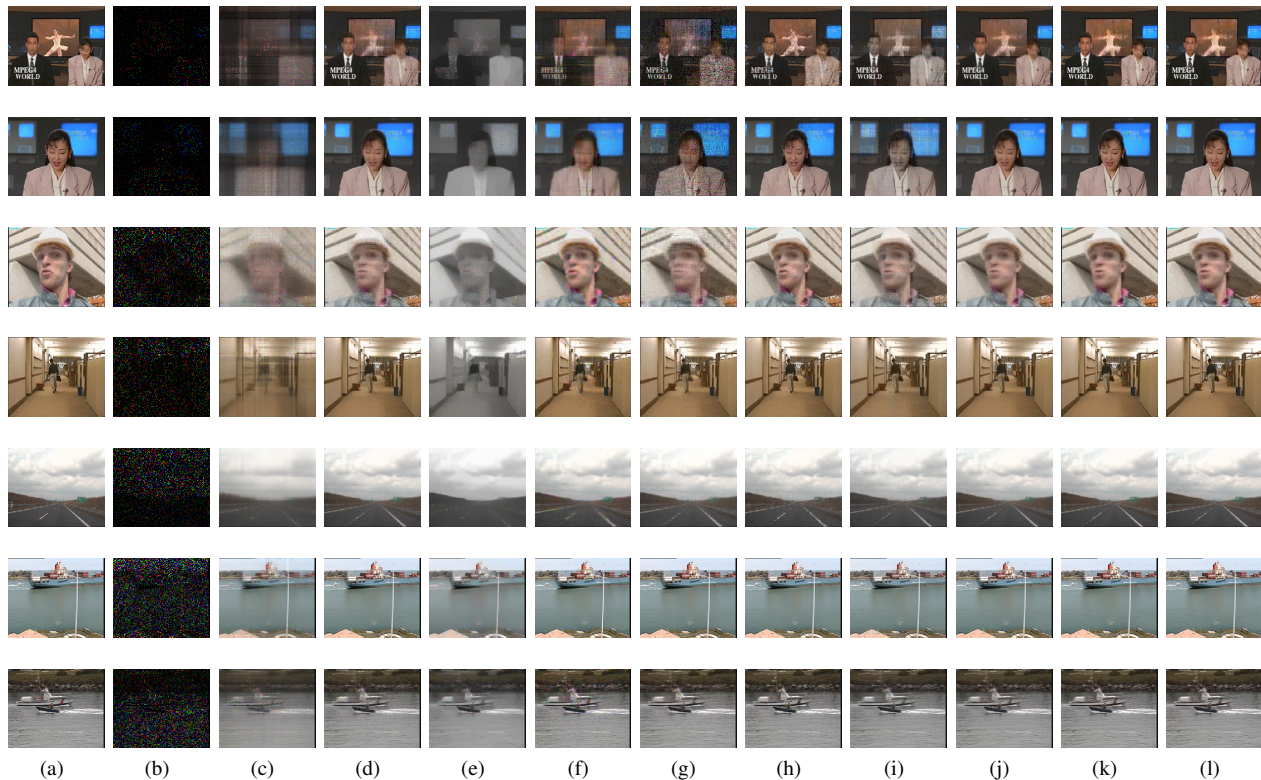


Fig. 4. (a) Original image. (b) Observed image. (c) HaLRTC. (d) TNN. (e) LRTC-TV-I. (f) McpTC. (g) PSTNN. (h) SMFLRTC. (i) FTNN. (j) WSTNN. (k) TEMCP1. (l) TEMCP2. SR: top 2 rows is 5%, middle 3 rows is 10% and last 2 rows is 20%. The rows of CVs are in order: the 44th frame of news, the 42th frame of akiyo, the 37th frame of foreman, the 26th frame of hall, the 28th frame of highway, the 15th frame of container, and the 10th frame of coastguard.

function, the tensor equivalent Minimax-Concave Penalty proposed by us is more efficient. On this basis, we give adaptive models for LRTC and TRPCA problems respectively. A large number of experiments show that the effects of the proposed TEMCP1 and TEMCP2 are basically the same, which is consistent with our theory. And our method can achieve better visual and numerical quantitative effects than contrast methods.

REFERENCES

- [1] Y.-M. Huang, H.-Y. Yan, Y.-W. Wen, and X. Yang, "Rank minimization with applications to image noise removal," *Information Sciences*, vol. 429, pp. 147–163, 2018.
- [2] B. Madathil and S. N. George, "Twist tensor total variation regularized-reweighted nuclear norm based tensor completion for video missing area recovery," *Information Sciences*, vol. 423, pp. 376–397, 2018.
- [3] Y. Wang, D. Meng, and M. Yuan, "Sparse recovery: from vectors to tensors," *National Science Review*, vol. 5, no. 5, pp. 756–767, 2018.
- [4] X.-L. Zhao, W.-H. Xu, T.-X. Jiang, Y. Wang, and M. K. Ng, "Deep plug-and-play prior for low-rank tensor completion," *Neurocomputing*, vol. 400, pp. 137–149, 2020.
- [5] S. Li, R. Dian, L. Fang, and J. M. Bioucas-Dias, "Fusing hyperspectral and multispectral images via coupled sparse tensor factorization," *IEEE Transactions on Image Processing*, vol. 27, no. 8, pp. 4118–4130, 2018.
- [6] X. Fu, W.-K. Ma, J. M. Bioucas-Dias, and T.-H. Chan, "Semiblind hyperspectral unmixing in the presence of spectral library mismatches," *IEEE Transactions on Geoscience and Remote Sensing*, vol. 54, no. 9, pp. 5171–5184, 2016.
- [7] J. Xue, Y. Zhao, W. Liao, and J. C.-W. Chan, "Nonlocal low-rank regularized tensor decomposition for hyperspectral image denoising,"

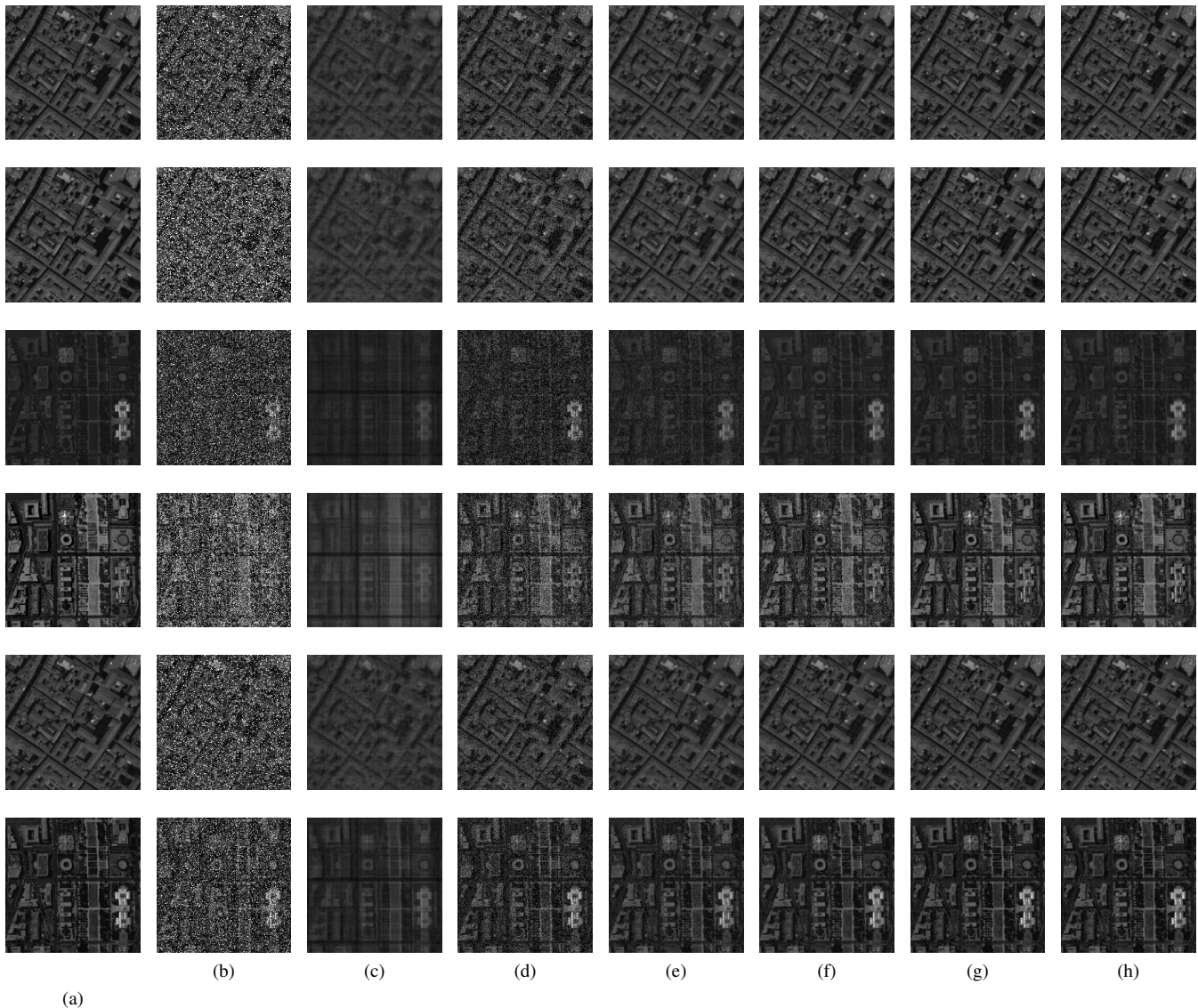


Fig. 5. (a) Original image. (b) Noise image. (c) SNN. (d) TNN. (e) 3DTNN. (f) 3DLogTNN. (g) TEMCP1. (h) TEMCP2.

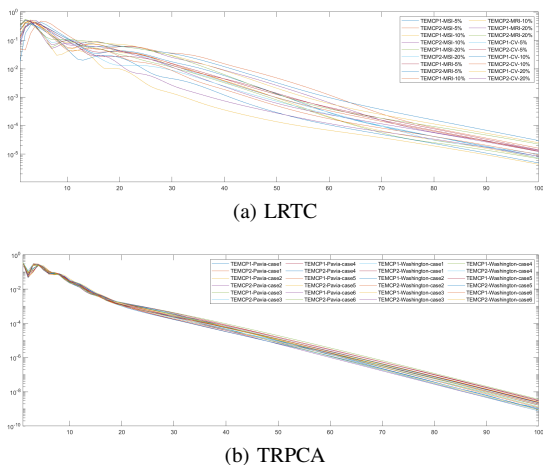


Fig. 6. The convergence behaviours of LRTC Algorithm, with respect to different sampling rates. The convergence behaviours of TRPCA Algorithm, with respect to different mixed noise.

- IEEE Transactions on Geoscience and Remote Sensing*, vol. 57, no. 7, pp. 5174–5189, 2019.
- [8] J. Xue, Y. Zhao, W. Liao, J. C.-W. Chan, and S. G. Kong, “Enhanced sparsity prior model for low-rank tensor completion,” *IEEE Transactions on Neural Networks and Learning Systems*, vol. 31, no. 11, pp. 4567–4581, 2020.
 - [9] H. Zhang, X. Liu, H. Fan, Y. Li, and Y. Ye, “Fast and accurate low-rank tensor completion methods based on qr decomposition and $l_{\{2, 1\}}$ norm minimization,” *arXiv preprint arXiv:2108.03002*, 2021.
 - [10] J.-H. Yang, X.-L. Zhao, T.-Y. Ji, T.-H. Ma, and T.-Z. Huang, “Low-rank tensor train for tensor robust principal component analysis,” *Applied Mathematics and Computation*, vol. 367, p. 124783, 2020.
 - [11] T.-X. Jiang, T.-Z. Huang, X.-L. Zhao, T.-Y. Ji, and L.-J. Deng, “Matrix factorization for low-rank tensor completion using framelet prior,” *Information Sciences*, vol. 436, pp. 403–417, 2018.
 - [12] M. Ding, T.-Z. Huang, T.-Y. Ji, X.-L. Zhao, and J.-H. Yang, “Low-rank tensor completion using matrix factorization based on tensor train rank and total variation,” *Journal of Scientific Computing*, vol. 81, no. 2, pp. 941–964, 2019.
 - [13] J. Xue, Y. Zhao, W. Liao, and J. Cheung-Wai Chan, “Nonconvex tensor rank minimization and its applications to tensor recovery,” *Information Sciences*, vol. 503, pp. 109–128, 2019.
 - [14] J. Xue, Y. Zhao, W. Liao, and J. Cheung-Wai Chan, “Total variation and rank-1 constraint rpca for background subtraction,” *IEEE Access*, vol. 6,

- pp. 49 955–49 966, 2018.
- [15] I. Kajo, N. Kamel, Y. Ruichek, and A. S. Malik, “Svd-based tensor-completion technique for background initialization,” *IEEE Transactions on Image Processing*, vol. 27, no. 6, pp. 3114–3126, 2018.
- [16] W. Cao, Y. Wang, J. Sun, D. Meng, C. Yang, A. Cichocki, and Z. Xu, “Total variation regularized tensor rpca for background subtraction from compressive measurements,” *IEEE Transactions on Image Processing*, vol. 25, no. 9, pp. 4075–4090, 2016.
- [17] W. Wei, L. Yi, Q. Xie, Q. Zhao, D. Meng, and Z. Xu, “Should we encode rain streaks in video as deterministic or stochastic?” in *2017 IEEE International Conference on Computer Vision (ICCV)*, 2017, pp. 2535–2544.
- [18] M. Li, Q. Xie, Q. Zhao, W. Wei, S. Gu, J. Tao, and D. Meng, “Video rain streak removal by multiscale convolutional sparse coding,” in *2018 IEEE/CVF Conference on Computer Vision and Pattern Recognition*, 2018, pp. 6644–6653.
- [19] Q. Zhao, L. Zhang, and A. Cichocki, “Bayesian cp factorization of incomplete tensors with automatic rank determination,” *IEEE Transactions on Pattern Analysis and Machine Intelligence*, vol. 37, no. 9, pp. 1751–1763, 2015.
- [20] T. Yokota, N. Lee, and A. Cichocki, “Robust multilinear tensor rank estimation using higher order singular value decomposition and information criteria,” *IEEE Transactions on Signal Processing*, vol. 65, no. 5, pp. 1196–1206, 2017.
- [21] E. Acar, D. M. Dunlavy, T. G. Kolda, and M. Mørup, “Scalable tensor factorizations for incomplete data,” *Chemometrics and Intelligent Laboratory Systems*, vol. 106, no. 1, pp. 41–56, 2011.
- [22] P. Tichavský, A.-H. Phan, and A. Cichocki, “Numerical cp decomposition of some difficult tensors,” *Journal of Computational and Applied Mathematics*, vol. 317, pp. 362–370, 2017.
- [23] Y.-F. Li, K. Shang, and Z.-H. Huang, “Low Tucker rank tensor recovery via admm based on exact and inexact iteratively reweighted algorithms,” *Journal of Computational and Applied Mathematics*, vol. 331, pp. 64–81, 2018.
- [24] X. Li, M. K. Ng, G. Cong, Y. Ye, and Q. Wu, “Mr-ntd: Manifold regularization nonnegative Tucker decomposition for tensor data dimension reduction and representation,” *IEEE Transactions on Neural Networks and Learning Systems*, vol. 28, no. 8, pp. 1787–1800, 2017.
- [25] Z. Zhang, G. Ely, S. Aeron, N. Hao, and M. Kilmer, “Novel methods for multilinear data completion and de-noising based on tensor-svd,” *2014 IEEE Conference on Computer Vision and Pattern Recognition*, pp. 3842–3849, 2014.
- [26] C. J. Hillar and L.-H. Lim, “Most tensor problems are np-hard,” *Journal of the ACM (JACM)*, vol. 60, no. 6, pp. 1–39, 2013.
- [27] Y.-B. Zheng, T.-Z. Huang, X.-L. Zhao, T.-X. Jiang, T.-Y. Ji, and T.-H. Ma, “Tensor n-tubal rank and its convex relaxation for low-rank tensor recovery,” *Information Sciences*, vol. 532, pp. 170–189, 2020.
- [28] I. Selesnick, “Sparse regularization via convex analysis,” *IEEE Transactions on Signal Processing*, vol. 65, no. 17, pp. 4481–4494, 2017.
- [29] B. K. Natarajan, “Sparse approximate solutions to linear systems,” *SIAM journal on computing*, vol. 24, no. 2, pp. 227–234, 1995.
- [30] B. Recht, M. Fazel, and P. A. Parrilo, “Guaranteed minimum-rank solutions of linear matrix equations via nuclear norm minimization,” *SIAM review*, vol. 52, no. 3, pp. 471–501, 2010.
- [31] C. Lu, C. Zhu, C. Xu, S. Yan, and Z. Lin, “Generalized singular value thresholding,” *Proceedings of the AAAI Conference on Artificial Intelligence*, vol. 29, no. 1, 2015.
- [32] Y. Hu, D. Zhang, J. Ye, X. Li, and X. He, “Fast and accurate matrix completion via truncated nuclear norm regularization,” *IEEE transactions on pattern analysis and machine intelligence*, vol. 35, no. 9, pp. 2117–2130, 2012.
- [33] P. K. Pokala, R. V. Hemadri, and C. S. Seelamantula, “Iteratively reweighted minimax-concave penalty minimization for accurate low-rank plus sparse matrix decomposition,” *IEEE Transactions on Pattern Analysis and Machine Intelligence*, 2021.
- [34] S. Boyd, N. Parikh, and E. Chu, *Distributed optimization and statistical learning via the alternating direction method of multipliers*. Now Publishers Inc, 2011.
- [35] Z. Lin, R. Liu, and Z. Su, “Linearized alternating direction method with adaptive penalty for low-rank representation,” *Advances in Neural Information Processing Systems*, vol. 24, pp. 612–620, 2011.
- [36] M. E. Kilmer and C. D. Martin, “Factorization strategies for third-order tensors,” *Linear Algebra and its Applications*, vol. 435, no. 3, pp. 641–658, 2011.
- [37] C. Lu, J. Feng, Y. Chen, W. Liu, Z. Lin, and S. Yan, “Tensor robust principal component analysis with a new tensor nuclear norm,” *IEEE Transactions on Pattern Analysis and Machine Intelligence*, vol. 42, no. 4, pp. 925–938, 2020.
- [38] C.-H. Zhang, “Nearly unbiased variable selection under minimax concave penalty,” *The Annals of statistics*, vol. 38, no. 2, pp. 894–942, 2010.
- [39] S. Wang, D. Liu, and Z. Zhang, “Nonconvex relaxation approaches to robust matrix recovery,” in *Twenty-Third International Joint Conference on Artificial Intelligence*, 2013.
- [40] S. Gu, L. Zhang, W. Zuo, and X. Feng, “Weighted nuclear norm minimization with application to image denoising,” in *Proceedings of the IEEE conference on computer vision and pattern recognition*, 2014, pp. 2862–2869.
- [41] H. Wang, F. Zhang, J. Wang, T. Huang, J. Huang, and X. Liu, “Generalized nonconvex approach for low-tubal-rank tensor recovery,” *IEEE Transactions on Neural Networks and Learning Systems*, pp. 1–15, 2021.
- [42] Z. Zhang and S. Aeron, “Exact tensor completion using t-svd,” *IEEE Transactions on Signal Processing*, vol. 65, no. 6, pp. 1511–1526, 2017.
- [43] Z. Wang, A. Bovik, H. Sheikh, and E. Simoncelli, “Image quality assessment: from error visibility to structural similarity,” *IEEE Transactions on Image Processing*, vol. 13, no. 4, pp. 600–612, 2004.
- [44] L. Zhang, L. Zhang, X. Mou, and D. Zhang, “Fsim: A feature similarity index for image quality assessment,” *IEEE Transactions on Image Processing*, vol. 20, no. 8, pp. 2378–2386, 2011.
- [45] L. Wald, *Data fusion: definitions and architectures: fusion of images of different spatial resolutions*. Presses des MINES, 2002.
- [46] J. Liu, P. Musialski, P. Wonka, and J. Ye, “Tensor completion for estimating missing values in visual data,” *IEEE Transactions on Pattern Analysis and Machine Intelligence*, vol. 35, no. 1, pp. 208–220, 2013.
- [47] X. Li, Y. Ye, and X. Xu, “Low-rank tensor completion with total variation for visual data inpainting,” *Proceedings of the AAAI Conference on Artificial Intelligence*, vol. 31, no. 1, 2017.
- [48] Q. Xie, Q. Zhao, D. Meng, and Z. Xu, “Kronecker-basis-representation based tensor sparsity and its applications to tensor recovery,” *IEEE Transactions on Pattern Analysis and Machine Intelligence*, vol. 40, no. 8, pp. 1888–1902, 2018.
- [49] T.-X. Jiang, T.-Z. Huang, X.-L. Zhao, and L.-J. Deng, “Multi-dimensional imaging data recovery via minimizing the partial sum of tubal nuclear norm,” *Journal of Computational and Applied Mathematics*, vol. 372, p. 112680, 2020.
- [50] T.-X. Jiang, M. K. Ng, X.-L. Zhao, and T.-Z. Huang, “Framelet representation of tensor nuclear norm for third-order tensor completion,” *IEEE Transactions on Image Processing*, vol. 29, pp. 7233–7244, 2020.
- [51] Y.-B. Zheng, T.-Z. Huang, X.-L. Zhao, T.-X. Jiang, T.-H. Ma, and T.-Y. Ji, “Mixed noise removal in hyperspectral image via low-fibered-rank regularization,” *IEEE Transactions on Geoscience and Remote Sensing*, vol. 58, no. 1, pp. 734–749, 2019.
- [52] W. Cao, Y. Wang, C. Yang, X. Chang, Z. Han, and Z. Xu, “Folded-concave penalization approaches to tensor completion,” *Neurocomputing*, vol. 152, pp. 261–273, 2015.
- [53] Y.-B. Zheng, T.-Z. Huang, T.-Y. Ji, X.-L. Zhao, T.-X. Jiang, and T.-H. Ma, “Low-rank tensor completion via smooth matrix factorization,” *Applied Mathematical Modelling*, vol. 70, pp. 677–695, 2019.
- [54] D. Goldfarb and Z. Qin, “Robust low-rank tensor recovery: Models and algorithms,” *SIAM Journal on Matrix Analysis and Applications*, vol. 35, no. 1, pp. 225–253, 2014.